OPEN ACCESS Freely available online

PLOS | ONE

Anti-Cancer Effects of REIC/Dkk-3-encoding Adenoviral Vector for the Treatment of Non-small Cell Lung Cancer

Kazuhiko Shien[1,2☯], Norimitsu Tanaka[2☯], Masami Watanabe[3,4,5], Junichi Soh[2], Masakiyo Sakaguchi[6], Keitaro Matsuo[7], Hiromasa Yamamoto[2], Masashi Furukawa[2], Hiroaki Asano[2], Kazunori Tsukuda[2], Yasutomo Nasu[3], Nam-Ho Huh[6], Shinichiro Miyoshi[2], Hiromi Kumon[3,5], Shinichi Toyooka[1,2*]

1 Department of Clinical Genomic Medicine, Okayama University Graduate School of Medicine, Dentistry and Pharmaceutical Sciences, Okayama, Japan, **2** Department of Thoracic Surgery, Okayama University Graduate School of Medicine, Dentistry and Pharmaceutical Sciences, Okayama, Japan, **3** Department of Urology, Okayama University Graduate School of Medicine, Dentistry and Pharmaceutical Sciences, Okayama, Japan, **4** Center for Gene and Cell Therapy, Okayama University Hospital, Okayama, Japan, **5** Innovation Center Okayama for Nanobio-Targeted Therapy (ICONT), Okayama University, Okayama, Japan, **6** Department of Cell Biology, Okayama University Graduate School of Medicine, Dentistry and Pharmaceutical Sciences, Okayama, Japan, **7** Department of Preventive Medicine, Kyusyu University Faculty of Medical Science, Fukuoka, Japan

Abstract

Objectives: REIC/Dkk-3 is down-regulated in a broad range of human cancer cells and is considered to function as a tumor suppressor. We previously reported that REIC/Dkk-3-expressing adenovirus vector (Ad-REIC) induced endoplasmic reticulum (ER) stress and cancer-specific apoptosis in human prostate cancer. In this study, we examined the therapeutic impact of Ad-REIC on non-small cell lung cancer (NSCLC).

Materials and Methods: We examined the anti-tumor effect of Ad-REIC on 25 NSCLC cell lines *in vitro* and A549 cells *in vivo*. Two of these cell lines were artificially established as EGFR-tyrosine kinase inhibitor (TKI) resistant sublines.

Results: Ad-REIC-treatment inhibited the cell viability by 40% or more in 13 (52%) of the 25 cell lines at multiplicity of infection (MOI) of 20 (20 MOI). These cell lines were regarded as being highly sensitive cells. The cell viability of a non-malignant immortalized cell line, OUMS-24, was not inhibited at 200 MOI of Ad-REIC. The effects of Ad-REIC on EGFR-TKI resistant sublines were equivalent to those in the parental cell lines. Here, we demonstrated that Ad-REIC treatment activated c-Jun N-terminal kinase (JNK) in NSCLC cell lines, indicating the induction of ER stress with GRP78/BiP (GRP78) up-regulation and resulting in apoptosis. A single intratumoral injection of Ad-REIC significantly inhibited the tumorigenic growth of A549 cells *in vivo*. As predictive factors of sensitivity for Ad-REIC treatment in NSCLC, we examined the expression status of GRP78 and coxsackievirus and adenovirus receptor (CAR). We found that the combination of the GRP78 and CAR expressional statuses may be used as a predictive factor for Ad-REIC sensitivity in NSCLC cells.

Conclusion: Ad-REIC induced JNK activation and subsequent apoptosis in NSCLC cells. Our study indicated that Ad-REIC has therapeutic potential against NSCLC and that the expression statuses of GRP78 and CAR may predict a potential therapeutic benefit of Ad-REIC.

Citation: Shien K, Tanaka N, Watanabe M, Soh J, Sakaguchi M, et al. (2014) Anti-Cancer Effects of REIC/Dkk-3-encoding Adenoviral Vector for the Treatment of Non-small Cell Lung Cancer. PLoS ONE 9(2): e87900. doi:10.1371/journal.pone.0087900

Editor: Sumitra Deb, Virginia Commonwealth University, United States of America

Received December 4, 2013; **Accepted** December 30, 2013; **Published** February 3, 2014

Funding: No current funding sources for this study.

Competing Interests: The authors have declared that no competing interests exist.

* E-mail: toyooka@md.okayama-u.ac.jp

☯ These authors contributed equally to this work.

Introduction

Lung cancer is the most common cause of death from cancer worldwide, and the metastatic form is a major factor leading to mortality [1]. There are two major histological subtypes of lung cancer: non-small cell lung cancer (NSCLC) and small cell lung cancer. Recent intensive studies have identified causative molecular alterations that have directly led to the development of new therapeutic strategies and have improved patient prognosis [2]. For example, mutations of the epidermal growth factor receptor gene (*EGFR*) are found in approximately 30% of NSCLCs, especially in lung adenocarcinomas, and EGFR-tyrosine kinase inhibitors (TKIs) are particularly effective in these tumors [3,4]. More recently, crizotinib has been shown to be effective for NSCLCs with an *EML4-ALK* fusion gene [5,6]. However, the number of patients with these alterations is limited, and little improvement in prognosis has been obtained in NSCLCs without these drug-sensitive alterations. Furthermore, acquired resistance eventually occurs in the majority of *EGFR*-mutant tumors, which had previously responded to EGFR-TKI, after an average of 10 months of treatment [7]. Thus, a new therapeutic modality is needed to improve the clinical outcome of patients with lung cancer.

REIC/Dkk-3, a member of the Dickkopf (Dkk) gene family, is originally found in immortalized cells and has been reported to be a tumor suppressor; its expression is significantly down-regulated in a broad range of cancer cell types, including lung cancer [8]. The heatmap image of messenger RNA (mRNA) expression of *REIC/Dkk-3* gene from the UCSC Cancer Genome Browse, which is freely available public database (https://genome-cancer.ucsc.edu/) (we downloaded the data on July 16 2013), showed that *REIC/Dkk-3* gene expression was reduced in majority of examined samples of both lung adenocarcinomas and squamous cell carcinomas compared with normal lung tissues (Figure S1). In addition, it could be confirmed from a public database that expression of *REIC/Dkk-3* was also low in many NSCLC cell lines (Gene Expression Omnibus repository [http://www.ncbi.nlm.nih.gov/geo, GEO accession GSE4824]). REIC/Dkk-3 is known to interfere with Wnt signaling via Wnt receptors [9,10] and was previously reported to play a distinct role in the induction of apoptosis and the inhibition of metastasis [11,12]. The induction of apoptosis in cancer cells is mainly caused by endoplasmic reticulum (ER) stress induced by the overproduction of REIC/Dkk-3 in the cells. ER stress triggers the activation of c-Jun N-terminal kinase (JNK), which is a critical event in apoptosis induced by the overproduction of REIC/Dkk-3 using an adenovirus vector (Ad-REIC) [11,13]. In our previous studies, we found that Ad-REIC had a therapeutic effect on various types of human cancer, including the prostate, testis, pleura, and breast carcinomas [11,13–15]. Ad-REIC infection and REIC/Dkk-3 protein are also known to up-regulate the anti-tumor immunosystem [16]. Based on preclinical data, a clinical trial using Ad-REIC for human prostate cancer has been ongoing in Japan and the USA (NCT01197209).

In this study, we investigated the therapeutic effect of Ad-REIC on NSCLC cells *in vitro* and *in vivo*. We also examined factors related to the sensitivity of cell lines to Ad-REIC as a step toward the development of customized Ad-REIC therapy for patients with NSCLC.

Materials and Methods

Ethics Statement

This study was carried out in strict accordance with the recommendations in the Guide for the Care and Use of Laboratory Animals of the National Institutes of Health. The protocol was approved by the Animal Care and Use Committee of Okayama University (Permit Number: OKU-2012-549). All surgery was performed under ketamine and xylazine anesthesia, and all efforts were made to minimize suffering.

Cell lines

Sixteen cell lines of human lung adenocarcinoma, 3 squamous cell carcinoma, 3 large cell carcinoma, 1 adenosquamous cell carcinoma, 2 EGFR-TKI-resistant sublines from HCC827 and PC-9 cells (HCC827-GR-high2 and RPC-9), the human mesothelioma cell line MSTO-211H (211H), and the normal human fibroblast cell line OUMS-24 were used in this study (Table 1). The details of cell lines used in this study are described in Method S1. The HCC827-GR-high2 and RPC-9 cell lines were established as described previously [17,18]. OUMS-24 was established at our institution [19].

Adenovirus vector carrying REIC/Dkk-3

REIC/Dkk-3 was overexpressed using an adenovirus (Ad-REIC) that we have previously generated [11]. A full-length cDNA of REIC/Dkk-3 was integrated into a cosmid vector pAxCAwt and transferred into an adenovirus vector by the COS-TPC method (Takara Bio, Shiga, Japan). An adenovirus vector carrying LacZ gene (Ad-LacZ) was also used as control [11].

Cell viability assay

Cells were plated in 96-well plates at a density of 1.5×10^3 cells/well at 48 h after infection with Ad-LacZ or Ad-REIC at a multiplicity of infection (MOI) of 20, 100, or 200 MOI. Cell viability was evaluated 3 days later using an MTS assay with CellTiter 96 Aqueous One Solution Reagent (Promega, Madison, WI).

Apoptosis assay

To examine the *in vitro* induction of apoptosis after treatment, we seeded the cells in 6-well plates and incubated them for 24 h. The cells were treated with Ad-LacZ or Ad-REIC at 20 MOI in serum-free medium (500 μL) for 2 h; the medium was then exchanged for fresh complete medium (2 mL). After an additional 48 h of incubation, Hoechst 33342 dye (Sigma-Aldrich, St. Louis, MO) was added to the medium at a concentration of 2 μg/mL, and the cells were incubated in the dark for 10 min. Hoechst 33342 is an intercalating dye that allows the determination of variations in the total chromatin quantity and the degree of chromatin condensation [15]. Using fluorescence microscopy, we identified apoptotic cells by the presence of highly condensed or fragmented nuclei. Apoptotic cells were counted in 5 different fields under microscopic observation.

Western blot analysis

The detailed protocol for the Western blot analysis is described in Method S1. It was performed under conventional conditions using the following antibodies: rabbit anti-human REIC/Dkk-3 antibody raised in our laboratory [11]; rabbit anti-human GRP78/BiP (GRP78) (ab21685; Abcam, Cambridge, MA); rabbit anti-human SAPK/JNK (#9252) and rabbit anti-human phospho-SAPK/JNK (Thr183/Tyr185; #9251) (Cell Signaling Technology, Beverly, MA); rabbit anti-human coxsackievirus and adenovirus receptor (CAR) (HPA030411; Atlas antibodies, Stockholm, Sweden); and mouse anti-actin (MAB1501; Millipore, Billerica, MA). The following secondary antibodies were used: goat anti-rabbit or anti-mouse IgG-conjugated horseradish peroxidase (Santa Cruz Biotechnology, Santa Cruz, CA). To detect the specific signals, the membranes were examined using ECL plus Western Blotting Detection Reagents (Amersham Biosciences UK Limited, Buckinghamshire, UK). In addition, the band intensities for GRP78, CAR, and actin, representing their expression levels, were measured using ImageQuant TL software (GE Healthcare Bioscience) and quantified by GRP78 or CAR/actin ratio.

Tumor growth assay in vivo

A549 cells (5×10^6 in 50 μL of phosphate buffered saline [PBS]) mixed with 50 μL of Matrigel (BD Biosciences, San Jose, CA) were subcutaneously injected into the right flank of adult female BALB/c nu/nu mice (CLEA Japan, Tokyo, Japan). The tumor volume was calculated using the empirical formula $V = 1/2\times[(\text{the shortest diameter})^2\times(\text{the longest diameter})]$. When the tumors had reached approximately 50–100 mm^3, mice (n = 15) were randomly divided into 3 treatment groups: (a) PBS; (b) Ad-LacZ; and (c) Ad-REIC. Viruses (1×10^9 pfu) in 100 μL of serum-free medium were administered intratumorally. At the end of experiments, mice were sacrificed after 24-days after the viral injection and tumors were harvested, measured, and photographed.

Table 1. Characteristics and the inhibition rate of cell viability on NSCLC cell lines.

Cell lines	Histological subtypes	Genetic alterations	Inhibition rate (%)			GRP78/Actin ratio (Low/High)	CAR/Actin ratio (Low/High)	Category
			20 MOI	100 MOI	200 MOI			
H2009	AD	*KRAS* mut	60	-	-	0.13 (Low)	0.73 (High)	A
H2228	AD	*EML4-ALK* fusion	60	-	-	0.27 (High)	0.70 (High)	B
HCC827	AD	*EGFR* mut	56	-	-	0.25 (High)	0.66 (High)	B
HCC827-GR-high2	AD	*EGFR* mut	55	-	-	0.12 (Low)	2.12 (High)	A
H2087	AD	*BRAF* mut	55	-	-	0.14 (Low)	1.22 (High)	A
HCC4006	AD	*EGFR* mut	54	-	-	0.15 (Low)	0.60 (High)	A
HCC4011	AD	*EGFR* mut	54	-	-	0.22 (Low)	0.13 (Low)	B
H522	AD	W/t	50	-	-	0.27 (High)	1.55 (High)	B
H157	SQ	*KRAS* mut	50	-	-	0.13 (Low)	0.98 (High)	A
A549	AD	*KRAS* mut	49	-	-	0.07 (Low)	0.55 (High)	A
H838	AD	W/t	47	-	-	0.10 (Low)	1.33 (High)	A
H1299	LC	*NRAS* mut	47	-	-	0.08 (Low)	0.68 (High)	A
H661	LC	W/t	40	-	-	0.42 (High)	1.89 (High)	B
H1819	AD	*HER2* amp	23	46	63	0.46 (High)	1.55 (High)	B
H1993	AD	W/t	22	32	40	0.69 (High)	0.09 (Low)	C
H441	AD	*KRAS* mutation	18	49	61	0.21 (Low)	0.17 (Low)	B
H2170	SQ	W/t	18	28	42	0.65 (High)	0.09 (Low)	C
HCC15	SQ	*HER4* mut	17	21	43	0.18 (Low)	0.12 (Low)	B
H460	LC	*KRAS, PIK3CA* mut	17	57	78	0.98 (High)	0.10 (Low)	C
PC-9	AD	*EGFR* mut	16	24	55	0.20 (Low)	0.16 (Low)	B
H1975	AD	*EGFR* mut	10	45	63	0.41 (High)	0.19 (Low)	C
HCC366	ADSQ	W/t	8	42	54	0.39 (High)	0.08 (Low)	C
RPC-9	AD	*EGFR* mut	4	15	40	0.24 (Low)	0.16 (Low)	B
H358	AD	*KRAS* mut	6	59	73	0.57 (High)	1.21 (High)	B
H3255	AD	*EGFR* mut	3	16	40	0.54 (High)	0.59 (High)	B
211H	MM	-	5	13	46	-	-	-
OUMS-24	NHF	-	5	0	0	-	-	-

NSCLC, non-small cell lung cancer; AD, adenocarcinoma; SQ, squamous cell carcinoma; LC, large cell carcinoma; ADSQ, adeno-squamous cell carcinoma; MM, malignant mesothelioma; NHF, normal human fibroblast; mut, mutation; W/t. wild type; MOI, multiplicity of infection.

doi:10.1371/journal.pone.0087900.t001

Statistical analyses

All data were analyzed using STATA ver.12 (STATA Corp., College Station, TX). Fisher's exact test was applied when appropriate. For a comparison of induction of apoptosis between Ad-REIC-treated and Ad-LacZ-treated A549 cells, a Cochran-Mantel-Haenszel statistics was applied for comparing. Repeated measurement ANOVA was applied for the comparison of xenotransplanted NSCLC tumor sizes among PBS, Ad-LacZ and Ad-REIC. $P<0.05$ was considered significant. All tests were two-sided.

Results

Effect of Ad-REIC on NSCLC cell lines

We examined the inhibition of cell viability using Ad-REIC and an MTS assay. In 13 (52%) of 25 NSCLC cell lines, Ad-REIC treatment at 20 MOI inhibited the cell viability (40%–60% inhibition), compared with Ad-LacZ treatment (Table 1, Figure 1). These cell lines were regarded as highly sensitive to Ad-REIC. In contrast, 12 cell lines (48%) were not inhibited by Ad-REIC treatment at 20 MOI and were regarded as resistant cells. OUMS-24 was not inhibited at 20 or 200 MOI of Ad-REIC. Of note, Ad-REIC treatment at 100 and 200 MOI improved the inhibition of cell viability (100 MOI: 15%–59% inhibition, 200 MOI: 40%–78% inhibition), compared with Ad-LacZ treatment (Table 1). Thus, we defined 20 MOI as a low MOI value and 200 MOI as a high MOI value. For comparison, Ad-REIC treatment was also performed in the human mesothelioma cell line 211H, which we previously reported to be Ad-REIC-sensitive [14]. The 211H was not inhibited at 20 MOI but was inhibited at 200 MOI of Ad-REIC (Table 1). The known molecular characteristics of each cell line are shown in Table 1. The 25 NSCLC cell lines consisted of 8 *EGFR*-mutant, 6 *KRAS*-mutant, 1 *HER4*-mutant, 1 *NRAS*-mutant, 1 *PIK3CA*-mutant, 1 *EML4-ALK* fusion, 1 *HER2*-amplified, and 6 cell lines without gene alterations listed. Nine of the 17 *EGFR*-wild type cell lines were sensitive to Ad-REIC. HCC827 and its resistant subline, HCC827-GR-high2, showed a similar degree of sensitivity to Ad-REIC. No trend in molecular genotype was seen between the sensitive and non-sensitive cell lines. These results suggested that the effect of Ad-REIC does not depend on a known molecular genotype.

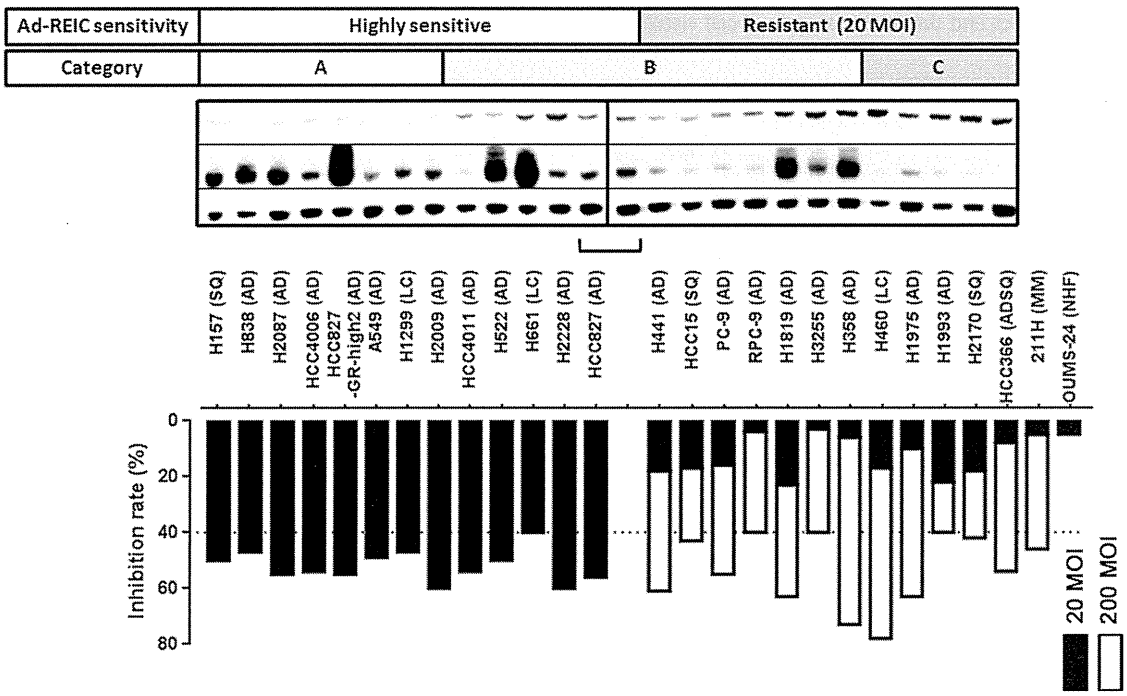

Figure 1. Sensitivity and predictive factors of sensitivity for Ad-REIC treatment in 25 NSCLC cell lines. The inhibition rates of 25 NSCLC cell lines transfected with Ad-REIC compared to Ad-LacZ are shown as black bar in 20 MOI and white bar in 200 MOI. Thirteen cell lines with over 40% inhibition rate in 20 MOI are defined as highly sensitive and 12 cell lines with lower inhibition rate in 20 MOI are defined as resistant. All the resistant cell lines shows over 40% inhibition rate in 200 MOI. The cell lines are classified into 3 categories based on the GRP and CAR protein expression level as follows; category A (low GRP/high CAR), category B (low GRP/low CAR or high GRP/high CAR), category C (high GRP/low CAR). All 8 highly sensitive cell lines were included in category A, and all 5 resistant cell lines were included in category C. Sq; squamous cell carcinoma, AD; adenocarcinoma, LC; large cell carcinoma, ADSQ; adenosquamous cell carcinoma, MM; malignant mesothelioma, NHF; normal human fibroblast.
doi:10.1371/journal.pone.0087900.g001

Hoechst 33342 staining was performed in A549 cells to examine the induction of apoptosis. Apoptotic cells were observed in Ad-REIC-treated A549 cells (Figure 2a). The mean rate of apoptosis was 22%, and it was significantly ($p<0.001$ by Cochran-Mantel-Haenszel test) increased in comparison with the control Ad-LacZ treatment.

The effect of recombinant REIC/Dkk-3 protein on NSCLC cell lines was examined in 7 randomly selected cell lines (NCI-H522, NCI-H611, NCI-H1299, NCI-H1819, NCI-H2009, PC-9, and A549). The MTS assay showed that REIC/Dkk-3 protein did not affect cell viability in the examined cell lines when administered at a concentration ranging from 1 to 200 μg/mL (data not shown).

Expression of GRP78 and CAR in response to Ad-REIC therapy

As predictive factors of Ad-REIC sensitivity in NSCLC, we examined the expressions of GRP78 and CAR; these expression statuses were correlated with the inhibition of cell viability by Ad-REIC in 13 cell lines. A previous study reported that the overexpression of GRP78 inhibited ER-stress, which may be oppositely correlated with the effect of Ad-REIC. CAR expression is tightly associated with the efficacy of adenovirus infection, which may be positively correlated with the effect of Ad-REIC. Western blotting was performed, and the expression level was quantified as shown in Table 1 and Figure 1. The median (range) of GRP78 and CAR expressions were 0.24 (0.075–0.98) and 0.60 (0.080–2.1), respectively. Based on these data, cells with a GRP78 expression level more than 0.25 were defined as High CRP78 expression, while those with a GRP78 less than 0.24 were defined as Low GRP78 expression. Regarding the CAR, 15 cell lines significantly high level of CAR expression (over 0.50) were defined as High CAR expression, while 10 cell lines those with significantly low level of CAR expression (under 0.20) were defined as Low CAR expression. GRP78 expression was low in 8 of the 13 Ad-REIC-sensitive cells (62%) and in 4 of the 12 Ad-REIC-resistant cells (33%). CAR expression was high in 12 of the 13 Ad-REIC-sensitive cells (92%) and in 3 of the 12 Ad-REIC-resistant cells (25%).

Next, we classified the cell lines into three categories based on the GRP78 and CAR expression statuses; cells with a Low GRP78/High CAR expression were classified as Category A, those with Low GRP78/Low CAR or High GRP78/High CAR expression were classified as Category B, and those with High GRP78/Low CAR expression were classified as Category C. The high sensitive cell rates were 100% in Category A (8 out of 8, 95% confidence interval [CI]: 63–100), 42% in Category B (5 out of 12, 95% CI: 15–72), and 0% in Category C (0 out of 5, 95% CI: 0–52) (Table 2). The categories were significantly associated with the sensitivity to Ad-REIC treatment ($p<0.01$).

JNK and GRP78 expression in NSCLC cell lines treated with Ad-REIC

A western blotting analysis demonstrated the significant expression of REIC/Dkk-3 protein in 14 NSCLC cell lines treated with Ad-REIC. In 9 cell lines infected with 20 MOI, Ad-REIC treatment resulted in the phosphorylation of JNK and the

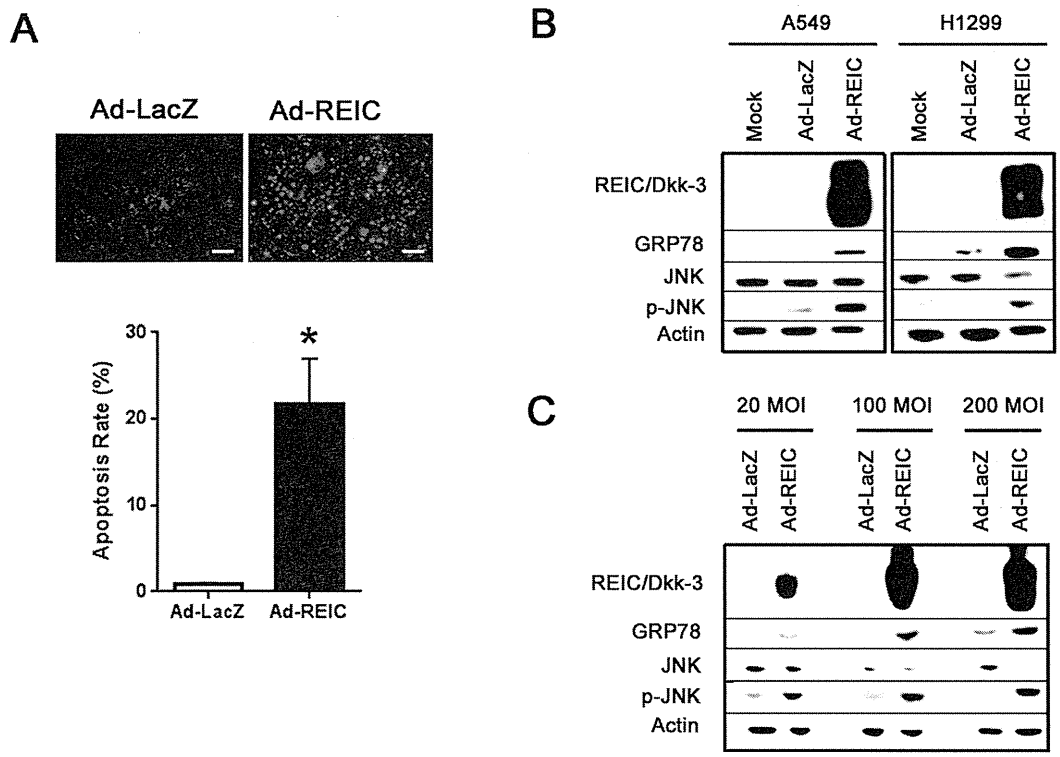

Figure 2. Ad-REIC induced JNK activation and subsequent apoptosis in NSCLC cells. (a) Induction of apoptosis after *in vitro* Ad-REIC treatment as examined in A549 cells using Hoechst 33342 staining. The upper panel indicates the appearance of apoptotic cells after Ad-REIC treatment. The lower panel shows the apoptotic rate of A549 cells after the indicated treatment. A total of 5 different fields were examined under a microscope to determine the apoptotic rate. A significant difference was observed (*$p<0.001$) between the Ad-LacZ and the Ad-REIC treatment. (bar: 100 μm) (b) Western blot analysis for proteins involved in signal transduction triggered by Ad-REIC. Cells were harvested at 48 h after transfection with Ad-LacZ or Ad-REIC at 20 MOI. (c) H460 cells, which are resistant to adenovirus transduction, were harvested at 48 h after transfection with Ad-LacZ or Ad-REIC at 20, 100, and 200 MOI.
doi:10.1371/journal.pone.0087900.g002

up-regulation of GRP78 (Figure 2b). In the other 8 cell lines, which were relatively resistant to Ad-REIC, the activation of JNK and GRP78 were observed at higher MOI values (100 and 200 MOI) (Figure 2c).

Effect of Ad-REIC on NSCLC tumors in a xenotransplantation model

We investigated the effect of Ad-REIC on the growth of A549 cells *in vivo*. One week after transplantation, when the tumor volume reached 50 to 100 mm^3, 1×10^9 plaque-forming units of Ad-REIC or Ad-LacZ in 100 μL of PBS or 100 μL of PBS alone were injected intratumorally. The tumors grew progressively in the PBS and Ad-LacZ treatment groups during the subsequent 24-day observation period. In contrast, the tumor growth in the Ad-REIC treatment group was significantly ($p<0.001$ by repeated measurement ANOVA) suppressed during the observation period (Figure 3a,b).

Table 2. Ad-REIC sensitivity and categories based on predictive factors.

(n)	Category A (8)	Category B (12)	Category C (5)
Highly sensitive (13)	8	5	0
Resistant in 20 MOI (12)	0	7	5

doi:10.1371/journal.pone.0087900.t002

Discussion

In the present study, we found that Ad-REIC was directly effective in more than half of the NSCLC cell lines that were examined, independent of its known driver alterations such as *EGFR* and *KRAS* mutations. An animal xenograft model also showed the therapeutic effect of Ad-REIC. The anti-tumor effect of Ad-REIC depends on ER-stress-mediated JNK activation loaded by the overproduction of REIC/Dkk-3 protein, resulting in the induction of apoptosis [14,20]. The activation of JNK, which is an essential step in the induction of ER stress and apoptosis by Ad-REIC, was observed at 20 MOI in NSCLC cell lines. On the other hand, the anti-tumor effect of recombinant REIC/Dkk-3 protein was not observed, as in other types of cancers that were previously examined. Originally, REIC/Dkk-3 was identified as a secretory protein and was assumed to exert a physiological function, but its cell surface receptor and its role as a secretory protein have not been identified.

We defined 20 MOI as a low MOI value and 200 MOI as a high MOI value because the normal human fibroblast cell line OUMS-24 was not inhibited at 20 or 200 MOI of Ad-REIC, whereas malignant cell lines were inhibited when the MOI value

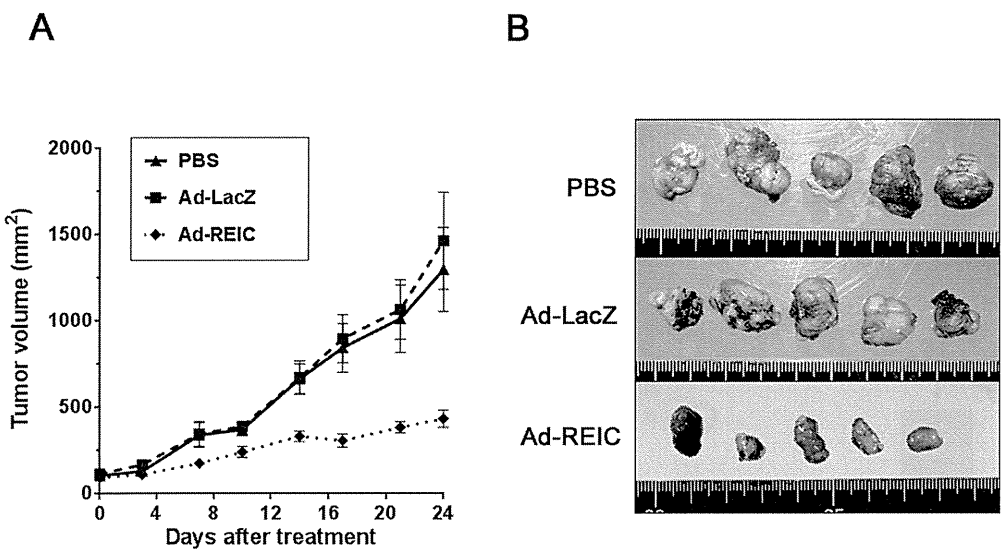

Figure 3. Anti-tumor effect of Ad-REIC treatment on A549 tumor growth *in vivo*. (a) The mean volume of the subcutaneous xenograft tumors was calculated for 5 mice in each group. A significant difference was observed between the results of Ad-REIC and Ad-LacZ treatment (*p< 0.001 by repeated measurement of ANOVA). (b) Appearance of the tumors at the time of sacrifice after treatment with PBS, Ad-LacZ, and Ad-REIC. doi:10.1371/journal.pone.0087900.g003

was elevated to 100 and 200 MOI in cell lines in which Ad-REIC had been ineffective at 20 MOI. In NSCLC, Ad-REIC was effective at a low MOI value in more than half of the cell lines that were tested. Considering the result that 211H was inhibited only at a high MOI value, Ad-REIC might be more effective in NSCLC than in mesothelioma.

Patient selection based on the molecular characteristics of tumor cells is an important theme for maximizing the therapeutic benefit and minimizing adverse effects. For this purpose, we focused on the GRP78 expression and CAR expression levels. GRP78 is a member of the Hsp70 family, which serves as an ER stress-signaling regulator [21]. A previous study showed that the overexpression of GRP78 conferred resistance to a wide variety of chemotherapeutic agents in various kinds of cells [22]. We also showed that the acquired resistance clone of PC-3 cells to Ad-REIC established after repeated exposure to Ad-REIC exhibited a high expression level of GRP78, compared with parental PC-3 cells [13]. Theoretically, Ad-REIC should be effective for tumor cells defined as Category A and not as effective for those defined as Category C. Although sensitive cells in Category B were identified, all 8 cells in Category A responded to Ad-REIC treatment. These results suggested that the expression statuses of GRP78 and CAR in tumors might be useful as biomarkers for customized Ad-REIC therapy in NSCLC while further confirmation is needed by a large scaled investigation using various kinds of cell lines.

As a recent topic of lung cancer treatment, EGFR-TKIs have been shown to be effective for the treatment of *EGFR*-mutant NSCLCs. However, acquired resistance to EGFR-TKIs after TKI treatment is a problem that needs to be overcome. In the current study, our results showed that the effect of Ad-REIC against acquired EGFR-TKI-resistant cells was equal to that against the parental cells, suggesting that Ad-REIC may be useful after the acquisition of resistance to EGFR-TKIs.

Although adenovirus vectors carrying appropriate tumor suppressor genes, such as REIC/Dkk-3, have great potential for cancer gene therapy, they do not exhibit target specificity and therefore may also infect normal cells in the vicinity of cancer cells. The authors reported that the infection of normal human fibroblasts (NHF) with Ad-REIC did not cause the apoptosis of NHF itself, but instead induced the production of interleukin (IL)-7. When Ad-REIC-infected NHF were mixed with untreated cancer cells and the mixture was transplanted into mice, the growth of the cancer cells was significantly suppressed, suggesting an indirect tumor-suppressive effect of Ad-REIC mediated by IL-7 [20]. These findings show that the mis-targeted infection of cancer stroma cells by Ad-REIC activates the immune system through the production of IL-7. In addition, the authors reported that REIC/Dkk-3 protein played a cytokine-like role in monocyte differentiation into dendritic-cell-like features *in vitro* and that the infiltration of CD11c- and CD8-positive (dendritic and killer T cell markers, respectively) cells was observed within the treated tumors *in vivo*. In the experiment using an orthotopic prostate tumor model with pre-established lung metastasis, the number of metastatic lung tumors significantly decreased after the injection of Ad-REIC at the primary tumor site in addition to the inhibition of the growth of orthotopic prostate tumors, suggesting that anti-cancer immune up-regulation by Ad-REIC treatment in primary tumor sites triggered anti-tumor effects even at distant tumor site [16]. These facts strongly suggest that REIC/Dkk-3 shows an indirect anti-tumor effect through the anti-tumor immune system that is an important factor in the treatment of metastatic disease. Because Ad-REIC has both direct and indirect effects on cancer therapy, it may become a powerful therapeutic option as a "one-bullet, two-arms" anti-cancer agent especially for NSCLCs, which often metastasize to other organs.

In regards to clinical usage, because our data suggest that CAR and GRP78 expression statuses in tumor cells predict the responsiveness of Ad-REIC treatment, Ad-REIC treatment should be preferentially performed for patients who are categorized as high sensitive group in early phase of treatment with low dose Ad-REIC. For patients whose tumor cells reveal intermediate or poor effectiveness with low dose Ad-REIC, it should be late phase in their treatment with high dose Ad-REIC. For these patients, cost effectiveness for treatment and clinical outcome should be

carefully considered. As for administration strategy, local administration might be preferable rather than systemic administration to minimize the adverse effect in clinical situations. We previously confirmed in mouse model that Ad-REIC could be widely distributed in the bodies after intratumoral local administration, and local administration was effective not only directly but also indirectly through the immune system effect [16,23]. In addition, intrapleural local administration could be another administration strategy for the patients with malignant pleural effusions. It has been reported that the intrapleural administration of adenoviral-mediated gene therapy is a useful approach for the generation of anti-tumor immune responses in malignant mesothelioma and metastatic pleural effusion in several clinical trials [24,25].

In conclusion, we demonstrated that Ad-REIC induced JNK activation and subsequent apoptosis in NSCLC cells irrespective of the type of known molecular alterations or the sensitivity to EGFR-TKI. The present study suggests that Ad-REIC has a therapeutic potential for NSCLC, and the expression statuses of GRP78 and CAR may be a predictor of Ad-REIC therapy.

Supporting Information

Figure S1 The heatmap image of mRNA expression of *REIC/Dkk-3* gene. The mRNA expression level of *REIC/Dkk-3* gene was obtained from the UCSC Cancer Genome Browse, which is freely available public database (https://genome-cancer.ucsc.edu/) (we downloaded the data on July 16 2013), showed that *REIC/Dkk-3* gene expression was reduced in majority of examined samples of both (a) lung adenocarcinomas and (b) squamous cell carcinomas, compared with normal lung tissues.
(PDF)

Method S1 Supporting information for cell lines and Western blot analysis.
(DOC)

Author Contributions

Conceived and designed the experiments: KS NT MW MS HY MF HA KT YN NHH SM HK ST. Performed the experiments: KS NT. Analyzed the data: KS NT JS KM HY ST. Contributed reagents/materials/analysis tools: KS NT MW MS KM YN NHH HK ST. Wrote the paper: KS NT JS HY ST.

References

1. Jemal A, Siegel R, Ward E, Hao Y, Xu J, et al. (2009) Cancer statistics, 2009. CA Cancer J Clin 59: 225–249.
2. Larsen JE, Cascone T, Gerber DE, Heymach JV, Minna JD (2011) Targeted therapies for lung cancer: clinical experience and novel agents. Cancer J 17: 512–527.
3. Shigematsu H, Lin L, Takahashi T, Nomura M, Suzuki M, et al. (2005) Clinical and biological features associated with epidermal growth factor receptor gene mutations in lung cancers. J Natl Cancer Inst 97: 339–346.
4. Tokumo M, Toyooka S, Kiura K, Shigematsu H, Tomii K, et al. (2005) The relationship between epidermal growth factor receptor mutations and clinicopathologic features in non-small cell lung cancers. Clin Cancer Res.
5. Kwak EL, Bang YJ, Camidge DR, Shaw AT, Solomon B, et al. (2010) Anaplastic lymphoma kinase inhibition in non-small-cell lung cancer. N Engl J Med 363: 1693–1703.
6. Shaw AT, Yeap BY, Solomon BJ, Riely GJ, Gainor J, et al. (2011) Effect of crizotinib on overall survival in patients with advanced non-small-cell lung cancer harbouring ALK gene rearrangement: a retrospective analysis. Lancet Oncol 12: 1004–1012.
7. Oxnard GR, Janjigian YY, Arcila ME, Sima CS, Kass SL, et al. (2011) Maintained sensitivity to EGFR tyrosine kinase inhibitors in EGFR-mutant lung cancer recurring after adjuvant erlotinib or gefitinib. Clin Cancer Res 17: 6322–6328.
8. Tsuji T, Miyazaki M, Sakaguchi M, Inoue Y, Namba M (2000) A REIC gene shows down-regulation in human immortalized cells and human tumor-derived cell lines. Biochem Biophys Res Commun 268: 20–24.
9. Krupnik VE, Sharp JD, Jiang C, Robison K, Chickering TW, et al. (1999) Functional and structural diversity of the human Dickkopf gene family. Gene 238: 301–313.
10. Mao B, Wu W, Davidson G, Marhold J, Li M, et al. (2002) Kremen proteins are Dickkopf receptors that regulate Wnt/beta-catenin signalling. Nature 417: 664–667.
11. Abarzua F, Sakaguchi M, Takaishi M, Nasu Y, Kurose K, et al. (2005) Adenovirus-mediated overexpression of REIC/Dkk-3 selectively induces apoptosis in human prostate cancer cells through activation of c-Jun-NH2-kinase. Cancer Res 65: 9617–9622.
12. Edamura K, Nasu Y, Takaishi M, Kobayashi T, Abarzua F, et al. (2007) Adenovirus-mediated REIC/Dkk-3 gene transfer inhibits tumor growth and metastasis in an orthotopic prostate cancer model. Cancer Gene Ther 14: 765–772.
13. Tanimoto R, Abarzua F, Sakaguchi M, Takaishi M, Nasu Y, et al. (2007) REIC/Dkk-3 as a potential gene therapeutic agent against human testicular cancer. Int J Mol Med 19: 363–368.
14. Kashiwakura Y, Ochiai K, Watanabe M, Abarzua F, Sakaguchi M, et al. (2008) Down-regulation of inhibition of differentiation-1 via activation of activating transcription factor 3 and Smad regulates REIC/Dickkopf-3-induced apoptosis. Cancer Res 68: 8333–8341.
15. Kawasaki K, Watanabe M, Sakaguchi M, Ogasawara Y, Ochiai K, et al. (2009) REIC/Dkk-3 overexpression downregulates P-glycoprotein in multidrug-resistant MCF7/ADR cells and induces apoptosis in breast cancer. Cancer Gene Ther 16: 65–72.
16. Watanabe M, Kashiwakura Y, Huang P, Ochiai K, Futami J, et al. (2009) Immunological aspects of REIC/Dkk-3 in monocyte differentiation and tumor regression. Int J Oncol 34: 657–663.
17. Shien K, Toyooka S, Yamamoto H, Soh J, Jida M, et al. (2013) Acquired Resistance to EGFR Inhibitors Is Associated with a Manifestation of Stem Cell-like Properties in Cancer Cells. Cancer Res 73: 3051–3061.
18. Kobayashi N, Toyooka S, Soh J, Yamamoto H, Dote H, et al. (2012) The anti-proliferative effect of heat shock protein 90 inhibitor, 17-DMAG, on non-small-cell lung cancers being resistant to EGFR tyrosine kinase inhibitor. Lung Cancer 75: 161–166.
19. Bai L, Mihara K, Kondo Y, Honma M, Namba M (1993) Immortalization of normal human fibroblasts by treatment with 4-nitroquinoline 1-oxide. Int J Cancer 53: 451–456.
20. Sakaguchi M, Kataoka K, Abarzua F, Tanimoto R, Watanabe M, et al. (2009) Overexpression of REIC/Dkk-3 in normal fibroblasts suppresses tumor growth via induction of interleukin-7. J Biol Chem 284: 14236–14244.
21. Kaufman RJ (2002) Orchestrating the unfolded protein response in health and disease. J Clin Invest 110: 1389–1398.
22. Li J, Lee AS (2006) Stress induction of GRP78/BiP and its role in cancer. Curr Mol Med 6: 45–54.
23. Sugimoto M, Watanabe M, Kaku H, Li SA, Noguchi H, et al. (2012) Preclinical biodistribution and safety study of reduced expression in immortalized cells/Dickkopf-3-encoding adenoviral vector for prostate cancer gene therapy. Oncol Rep 28: 1645–1652.
24. Sterman DH, Recio A, Carroll RG, Gillespie CT, Haas A, et al. (2007) A phase I clinical trial of single-dose intrapleural IFN-beta gene transfer for malignant pleural mesothelioma and metastatic pleural effusions: high rate of antitumor immune responses. Clin Cancer Res 13: 4456–4466.
25. Sterman DH, Recio A, Haas AR, Vachani A, Katz SI, et al. (2010) A phase I trial of repeated intrapleural adenoviral-mediated interferon-beta gene transfer for mesothelioma and metastatic pleural effusions. Mol Ther 18: 852–860.

DOI:10.1093/jnci/djt338
Advance Access publication December 7, 2013

BRIEF COMMUNICATION

Novel Germline Mutation in the Transmembrane Domain of *HER2* in Familial Lung Adenocarcinomas

Hiromasa Yamamoto, Koichiro Higasa, Masakiyo Sakaguchi, Kazuhiko Shien, Junichi Soh, Koichi Ichimura, Masashi Furukawa, Shinsuke Hashida, Kazunori Tsukuda, Nagio Takigawa, Keitaro Matsuo, Katsuyuki Kiura, Shinichiro Miyoshi, Fumihiko Matsuda, Shinichi Toyooka

Manuscript received July 7, 2013; revised October 14, 2013; accepted October 16, 2013.

Correspondence to: Shinichi Toyooka, MD, PhD, Okayama University Graduate School of Medicine, Dentistry and Pharmaceutical Sciences, Clinical Genomic Medicine/Thoracic, Breast and Endocrinological Surgery, 2-5-1 Shikata-cho, Kita-ku, Okayama, Okayama 700–8558, Japan (e-mail: toyooka@md.okayama-u.ac.jp).

We encountered a family of Japanese descent in which multiple members developed lung cancer. Using whole-exome sequencing, we identified a novel germline mutation in the transmembrane domain of the human epidermal growth factor receptor 2 (*HER2*) gene (G660D). A novel somatic mutation (V659E) was also detected in the transmembrane domain of *HER2* in one of 253 sporadic lung adenocarcinomas. Because the transmembrane domain of *HER2* is considered to be responsible for the dimerization and subsequent activation of the *HER* family and downstream signaling pathways, we performed functional analyses of these *HER2* mutants. Mutant HER2 G660D and V659E proteins were more stable than wild-type protein. Both the G660D and V659E mutants activated Akt. In addition, they activated p38, which is thought to promote cell proliferation in lung adenocarcinoma. Our findings strongly suggest that mutations in the transmembrane domain of *HER2* may be oncogenic, causing hereditary and sporadic lung adenocarcinomas.

J Natl Cancer Inst (2014) 106(1): djt338

Familial lung cancers are rare among human malignancies. Recent studies have reported that germline mutations in the epidermal growth factor receptor (*EGFR*) gene predispose the development of lung cancer. Reported familial lung adenocarcinomas with a germline *EGFR* mutation, such as T790M, carry secondary somatic *EGFR* mutations, including exon 19 deletion and exon 21 L858R mutation (1–4). We encountered a family of Japanese descent in which multiple members developed lung cancer (Figure 1). The proband (III-4) was a 53-year-old woman with multiple lung adenocarcinomas in bilateral lungs. She was a light smoker with a 1.2-pack-year history of smoking. She had undergone a left lower lobectomy for multiple lung adenocarcinomas at the age of 44 years. Her mother (II-4), a never smoker, also had multiple lung adenocarcinomas. Partial pulmonary resections of two tumors were performed for II-4 for the purpose of diagnosis after pleural dissemination was found during surgery, and multiple lesions were removed in a lobectomy or partial resections in III-4. A histological examination of the resected tumors in II-4 revealed nonmucinous adenocarcinoma in situ and nonmucinous minimally invasive adenocarcinoma, whereas

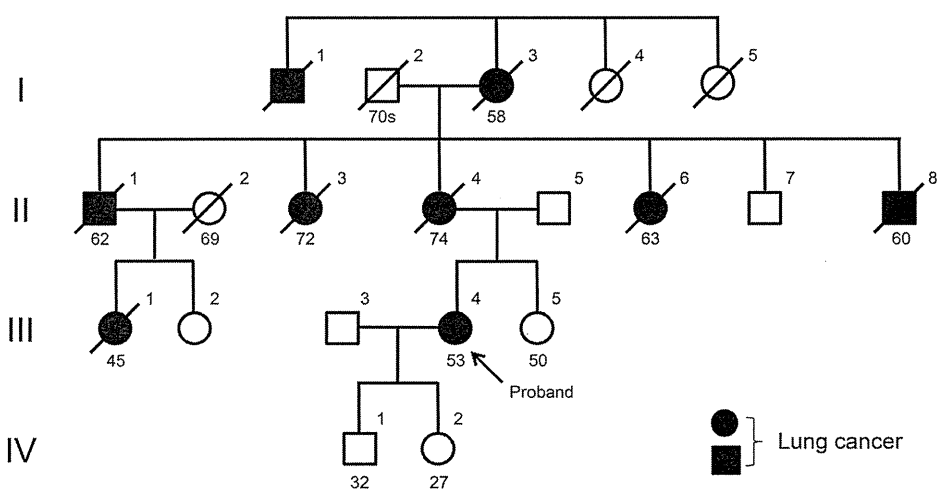

Figure 1. Pedigree chart of a Japanese family in which multiple members developed lung cancer. The **boxes** and **circles** indicate men and women, respectively. The **numbers** at the bottom of each member indicate the age at the time of death or the time of the analysis. An **oblique line** shows deceased family members. The proband (III-4) had multiple lung adenocarcinomas (**arrow**). Tumor tissue, nonmalignant lung tissue, and peripheral blood samples were obtained from III-4. The proband's mother (II-4) also had multiple lung adenocarcinomas, and tumor and nonmalignant lung tissue samples were available. The proband's father (II-5) and sister (III-5) were both unaffected, and peripheral blood samples were obtained from these individuals. Some family members who were not considered as critical for this study were excluded from the pedigree chart to preserve confidentiality. Whole-exome sequencing was performed for individuals II-4, II-5, III-4, and III-5.

the histological findings of pleural dissemination indicated mucus-containing adenocarcinoma. Those of III-4 contained various subtypes of adenocarcinoma, including nonmucinous and mucinous adenocarcinoma in situ and invasive mucinous adenocarcinoma. In addition, normal-appearing lung parenchyma obtained from a lobectomy in III-4 revealed innumerable small preinvasive lesions, implying the presence of precancerous changes throughout the lung (Supplementary Figure 1, available online). Sequencing analyses of *EGFR* exons 18 to 21 and *KRAS* as well as an immunohistochemical staining for ALK protein in the resected tumors indicated no genetic alterations in these genes. The pedigree chart suggested that lung cancer was inherited in an autosomal dominant manner.

After obtaining permission from the Institutional Review Board at Okayama University Hospital and informed consent from the patients and other family members, we performed a whole-exome sequencing study. Tumor DNA samples from II-4, tumor and peripheral blood DNA samples from III-4, and peripheral blood DNA samples from two unaffected family members (II-5 and III-5) were used for the analysis. The candidate germline alterations were restricted to 29 variants by comparing the whole-exome sequencing results between the patients and the unaffected family members. Among them, we focused on a point mutation in the human epidermal growth factor receptor 2 (*HER2/neu*) gene (NM_004448, G660D, GGC to GAC), which was located in exon 17 encoding the transmembrane domain of *HER2* (Supplementary Tables 1–3). This alteration was confirmed by direct sequencing (Figure 2A). We also confirmed that there was no copy number gain of *HER2* in the examined tumors based on the degree of read-depth in the whole-exome sequencing results. Of note, no mutations in genes known to cause lung cancers were detected for tumors from III-4 and II-4.

We considered that somatic mutations in the *HER2* transmembrane domain might act as driver mutations in lung cancer. Hence, we sequenced exon 17 of the *HER2*

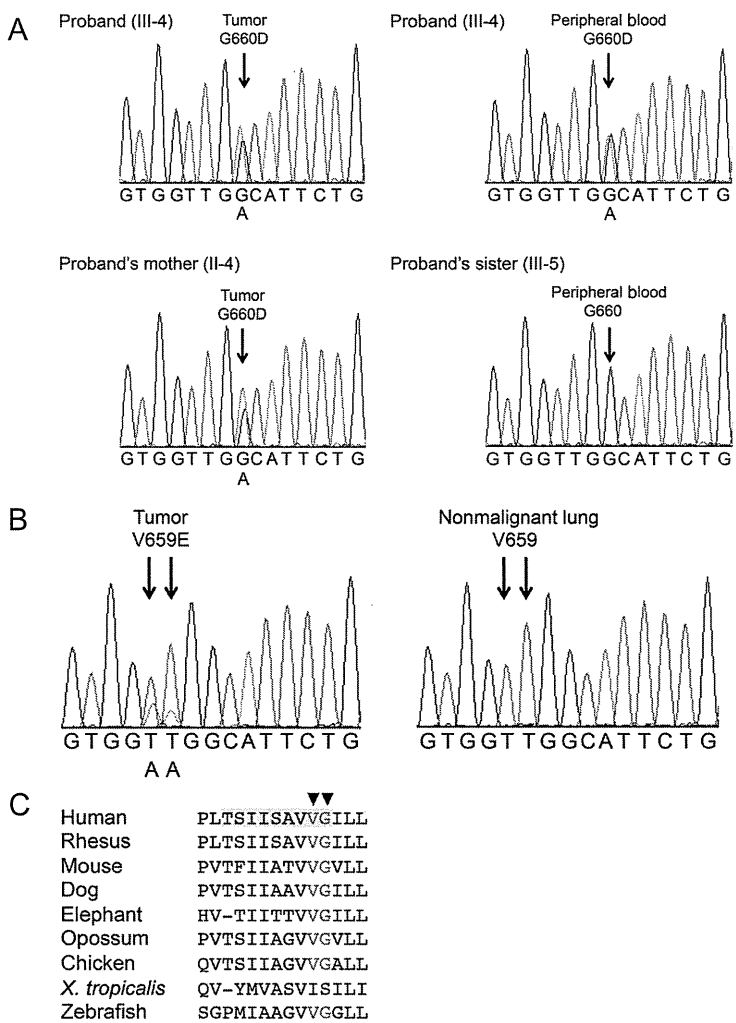

Figure 2. DNA and amino acid sequences in the transmembrane domain of *HER2*. **A**) Direct Sanger sequencing of the proband (III-4), her affected mother (II-4), and her unaffected sister (III-5). The results indicated that G660D was a germline mutation. **B**) Direct sequencing of a sporadic lung adenocarcinoma with a *HER2* V659E mutation. V659E was found to be of somatic origin based on the sequencing results of the peritumoral lung tissue from the same specimen. All the sequence variants were confirmed by independent polymerase chain reaction amplifications and were sequenced in both directions. **C**) Interspecies conservation of the transmembrane domain of *HER2* (UCSC Genome Browser, http://genome.ucsc.edu, accessed September 12, 2013). The **yellow highlight** indicates the N-terminal glycine zipper motif Thr^{652}-X_3-Ser^{656}-X_3-Gly^{660}, a tandem variant of a GG4-like motif of human *HER2*. Codons 659 and 660 in human *HER2* are highly conserved among the listed vertebrate species (shown in **red**). *X. tropicalis* = *Xenopus tropicalis*.

in the tumor samples of 315 sporadic non–small cell lung cancer patients, of which 253 were adenocarcinomas. Although the *HER2* G660D mutation was not detected, a novel nonsynonymous mutation, V659E (GTT to GAA), next to codon 660 was identified in one of these patients. This patient was histologically diagnosed as nonmucinous adenocarcinoma in situ, and the patient had neither smoking history nor apparent family history of lung cancer. This V659E mutation was certainly a somatic mutation because it was not identified in the peritumoral lung tissue of the same patient (Figure 2B). The alignment of *HER2* amino acid sequences showed high conservation of valine 659 and glycine 660 among vertebrates (Figure 2C).

HER2 somatic mutations have been reported in 2% to 4% of lung adenocarcinomas (5–7). However, all reported mutations were restricted to its tyrosine kinase domain (6,7). According to the cBioPortal for Cancer Genomics (http://www.cbioportal.org/public-portal/, accessed September 12, 2013), the same genetic mutation in the *HER2* has not been reported in any type of cancer. Interestingly, a previous study reported that a mutation in the transmembrane domain (V664E) of the rat *neu* gene, which corresponds to V659E in its human homolog *HER2*, induced oncogenic transformation (8). In addition, in vivo experiments showed that the *HER2* V659E mutation contributed to the stability of HER2 dimers, resulting in the dysregulated receptor activation and subsequent cell transformation (9,10). Furthermore, the novel mutations were located within the glycine zipper motif Thr^{652}-X_3-Ser^{656}-X_3-Gly^{660}, a tandem variant of the GG4-like motif, at the N-terminal portion of the transmembrane domain, which was critically related to the dimerization of HER2 (Figure 2C) (9,11). Accordingly, we performed a functional analysis of the mutant HER2 proteins. We found that the degradation of HER2 protein after the administration of cycloheximide was slower in G660D and V659E mutants as compared with wild-type (Supplementary Figure 2A), indicating the higher stability of the mutant proteins than wild-type protein. In addition, results of a phospho-mitogen–activated protein kinase array indicated the activation of Akt and p38α (data not shown). Indeed, Akt is known to be activated by HER2 by phosphatidylinositol 3-kinase and leads to increased cell growth and survival (12,13). Also, the activation of p38 was shown to contribute to the viability of lung adenocarcinoma cells derived from never or light smokers (14,15). A western blot analysis for Akt and p38 successfully confirmed the upregulation of both phospho-Akt and phospho-p38 expression in the mutant *HER2* transfectants (Supplementary Figure 2B).

Because the G660D alteration in *HER2* might have been the cause of the lung cancer in the pedigree studied, we investigated whether familial aggregation of cancer in other organs could be seen in this pedigree. We found that II-1 and II-6 developed renal and gastric cancers, respectively; however, both of them also had lung cancer. The reason why other types of clinically apparent malignances were rarely found in this pedigree is unclear. The G660D germline mutation may be tolerated in organs other than the lung.

This study had some limitations. First, the carcinogenic potential of the *HER2* mutation at the transmembrane domain should be confirmed in other models such as transgenic mice. Second, the rarity of these mutations in sporadic lung cancers may be the limitation for generalizability to other cases even if targeting therapies for similar types of *HER2* mutation were developed.

In conclusion, we identified a novel germline mutation in the transmembrane domain of the *HER2* in familial lung adenocarcinomas. Somatic mutation in the *HER2* transmembrane domain may be a possible cause of sporadic lung adenocarcinomas.

References

1. Bell DW, Gore I, Okimoto RA, et al. Inherited susceptibility to lung cancer may be associated with the T790M drug resistance mutation in EGFR. *Nat Genet*. 2005;37(12):1315–1316.
2. Ikeda K, Nomori H, Mori T, Sasaki J, Kobayashi T. Novel germline mutation: EGFR V843I in patient with multiple lung adenocarcinomas and family members with lung cancer. *Ann Thorac Surg*. 2008;85(4):1430–1432.
3. Ohtsuka K, Ohnishi H, Kurai D, et al. Familial lung adenocarcinoma caused by the EGFR V843I germ-line mutation. *J Clin Oncol*. 2011;29(8):e191–e192.
4. van Noesel J, van der Ven WH, van Os TA, et al. Activating germline R776H mutation in the epidermal growth factor receptor associated with lung cancer with squamous differentiation. *J Clin Oncol*. 2013;31(10):e161–e164.
5. Pao W, Girard N. New driver mutations in non-small-cell lung cancer. *Lancet Oncol*. 2011;12(2):175–180.
6. Shigematsu H, Takahashi T, Nomura M, et al. Somatic mutations of the HER2 kinase domain in lung adenocarcinomas. *Cancer Res*. 2005;65(5):1642–1646.
7. Stephens P, Hunter C, Bignell G, et al. Lung cancer: intragenic ERBB2 kinase mutations in tumours. *Nature*. 2004;431(7008):525–526.
8. Bargmann CI, Hung MC, Weinberg RA. Multiple independent activations of the neu oncogene by a point mutation altering the transmembrane domain of p185. *Cell*. 1986;45(5):649–657.
9. Bocharov EV, Mineev KS, Volynsky PE, et al. Spatial structure of the dimeric transmembrane domain of the growth factor receptor ErbB2 presumably corresponding to the receptor active state. *J Biol Chem*. 2008;283(11):6950–6956.
10. Fleishman SJ, Schlessinger J, Ben-Tal N. A putative molecular-activation switch in the transmembrane domain of erbB2. *Proc Natl Acad Sci U S A*. 2002;99(25):15937–15940.
11. Mineev KS, Bocharov EV, Pustovalova YE, Bocharova OV, Chupin VV, Arseniev AS. Spatial structure of the transmembrane domain heterodimer of ErbB1 and ErbB2 receptor tyrosine kinases. *J Mol Biol*. 2010;400(2):231–243.
12. Baselga J, Swain SM. Novel anticancer targets: revisiting ERBB2 and discovering ERBB3. *Nat Rev Cancer*. 2009;9(7):463–475.
13. Engelman JA. Targeting PI3K signalling in cancer: opportunities, challenges and limitations. *Nat Rev Cancer*. 2009;9(8):550–562.
14. Mountzios G, Planchard D, Besse B, et al. Mitogen-activated protein kinase activation in lung adenocarcinoma: a comparative study between ever smokers and never smokers. *Clin Cancer Res*. 2008;14(13):4096–4102.
15. Planchard D, Camara-Clayette V, Dorvault N, Soria JC, Fouret P. p38 Mitogen-activated protein kinase signaling, ERCC1 expression, and viability of lung cancer cells from never or light smoker patients. *Cancer*. 2012;118(20):5015–5025.

Funding

This study was supported by a Grant-in Aid for Scientific Research from the Ministry of Education, Culture, Sports, Science and Technology of Japan (25293302 to ST).

Note

H. Yamamoto, J. Soh, S. Miyoshi, and S. Toyooka conceived the project. K. Higasa, M. Sakaguchi, K. Shien, and K. Ichimura performed the experiments. H. Yamamoto, J. Soh, M. Furukawa, S. Hashida, N. Takigawa, K. Kiura, K. Tsukuda, and S. Toyooka collected the samples and assisted with the experiments. H. Yamamoto, K. Higasa, K. Shien, and K. Matsuo analyzed the data. H. Yamamoto, K. Higasa, M. Sakaguchi, F. Matsuda, and S. Toyooka prepared the manuscript with input from the other authors. S. Miyoshi, F. Matsuda, and S. Toyooka supervised the project. The authors declared no conflicts of interest.

Affiliations of authors: Department of Thoracic, Breast and Endocrinological Surgery (HY, KS, JS, MF, SH, KT, SM, ST), Department of Clinical Genomic Medicine (KS, ST), Department of Cell Biology (MS), Department of Pathology (KI), and Department of Hematology, Oncology and Respiratory Medicine (KK), Okayama University Graduate School of Medicine, Dentistry and Pharmaceutical Sciences, Okayama, Japan; Center for Genomic Medicine, Kyoto University School of Medicine, Kyoto, Japan (KH, FM); Department of General Internal Medicine 4, Kawasaki Medical School, Okayama, Japan (NT); Department of Preventive Medicine, Kyushu University Faculty of Medical Sciences, Fukuoka, Japan (KM).

Lung Cancer 82 (2013) 485–490

Contents lists available at ScienceDirect

Lung Cancer

journal homepage: www.elsevier.com/locate/lungcan

The degree of microRNA-34b/c methylation in serum-circulating DNA is associated with malignant pleural mesothelioma

Takayuki Muraoka[a], Junichi Soh[a], Shinichi Toyooka[a,*], Keisuke Aoe[b], Nobukazu Fujimoto[c], Shinsuke Hashida[a], Yuho Maki[a], Norimitsu Tanaka[a], Kazuhiko Shien[a], Masashi Furukawa[a], Hiromasa Yamamoto[a], Hiroaki Asano[a], Kazunori Tsukuda[a], Takumi Kishimoto[c], Takemi Otsuki[d], Shinichiro Miyoshi[a]

[a] Department of Thoracic Surgery, Graduate School of Medicine, Dentistry and Pharmaceutical Sciences, Okayama University, 2-5-1 Shikata-cho, Kita-ku, Okayama 700-8558, Japan
[b] Department of Medical Oncology and Clinical Research, National Hospital Organization, Yamaguchi-Ube Medical Center, 685 Higashi-kiwa, Ube 755-0241, Japan
[c] Department of Respiratory Medicine, Okayama Rosai Hospital, 1-10-25 Chikkomidorimachi, Minami-ku, Okayama 702-8055, Japan
[d] Department of Hygiene, Kawasaki Medical School, 577 Matsushima, Kurashiki 701-0192, Japan

ARTICLE INFO

Article history:
Received 29 May 2013
Received in revised form
18 September 2013
Accepted 29 September 2013

Keywords:
Digital PCR
Malignant pleural mesothelioma
microRNA
miR-34b/c
Methylation
Circulating DNA

ABSTRACT

Objectives: Malignant pleural mesothelioma (MPM) is an aggressive tumor with a poor prognosis. microRNA-34b/c (miR-34b/c), which plays an important role in the pathogenesis of MPM, is frequently downregulated by DNA methylation in approximately 90% of MPM cases. In this study, we estimated the degree of miR-34b/c methylation in serum-circulating DNA using a digital methylation specific PCR assay (MSP).

Materials and methods: A real-time MSP assay was performed using the SYBR Green method. The melting temperature (Tm) of each PCR product was examined using a melting curve analysis. For a digital MSP assay, 40 wells were analyzed per sample. A total of 110 serum samples from 48 MPM cases, 21 benign asbestos pleurisy (BAP) cases, and 41 healthy volunteers (HVs) were examined.

Results: Positive range of Tm value for miR-34b/c methylation was defined as 77.71–78.79 °C which was the mean ± 3 standard deviations of 40 wells of a positive control. The number of miR-34b/c methylated wells was counted per sample according to this criterion. The number of miR-34b/c methylated wells in MPM cases was significantly higher than that in BAP cases ($P = 0.03$) or HVs ($P < 0.001$). Advanced MPM cases tended to have higher number of miR-34b/c methylated wells than early MPM cases. Receiver–operating characteristic (ROC) curve analysis revealed that three number of miR-34b/c methylated wells per sample was the best cut-off of positivity of MPM with a 67% of sensitivity and a 77% specificity for prediction. The area under the ROC curve was 0.77.

Conclusions: Our digital MSP assay can quantify miR-34b/c methylation in serum-circulating DNA. The degree of miR-34b/c methylation in serum-circulating DNA is associated with MPM, suggesting that this approach might be useful for the establishment of a new detection system for MPM.

1. Introduction

Asbestos exposure has been reported to cause asbestos-related diseases such as malignant pleural mesothelioma (MPM), primary lung cancer, and benign asbestos pleurisy (BAP) [1]. Although the use of asbestos has been strictly restricted, the number of MPM patients who had been exposed to asbestos is still increasing [2,3]. MPM is an aggressive tumor with a dismal prognosis, with a median overall survival period of 12 months [2]. Approximately 85–90% of patients with MPM present with unresectable disease at the time of diagnosis [4]. Additionally, both MPM and BAP cases suffer from common symptoms caused by pleural effusion. These conditions are difficult to distinguish using not only radiological imaging tests such as chest X-ray and computed tomography, but also cytological examinations of pleural effusion [5,6]. Therefore, pathological validation by means of an invasive pleural biopsy with a full-layer resection of the parietal pleura is strongly recommended [7], although the possibility of a sampling error at the time of biopsy is significant; whether a few pieces of the parietal pleura are actually representative of the entire pleural lesion is unclear [8].

* Corresponding author. Tel.: +81 86 235 7265; fax: +81 86 235 7269.
E-mail address: toyooka@md.okayama-u.ac.jp (S. Toyooka).

0169-5002/$ – see front matter © 2013 Elsevier Ireland Ltd. All rights reserved.
http://dx.doi.org/10.1016/j.lungcan.2013.09.017

Considering the difficulty associated with the pathological diagnosis of MPM, a definitive diagnosis based on pathological finding alone is occasionally challenging [9,10]. Since misguided diagnoses lead to delays in treatment and early diagnosis and subsequent treatment are thought to improve the clinical outcome of patients with MPM, a critical need exists for the development of a reliable and non-invasive test for the detection of MPM.

Reportedly, the downregulation of several tumor suppressive genes, such as *BMP3b* [11], *BMP6* [11], *IGFBP* [12], and *RASSF1A* [13], frequently occurs as a result of DNA methylation in MPM cases. Similar to protein coding genes, microRNAs (miRs), which are a group of non-coding small RNAs that mostly regulate their target messenger-RNAs through posttranscriptional repression [14], are downregulated through the methylation of their promoter regions [15]. In fact, we have recently revealed that miR-34b/c, which plays an important role in the pathogenesis of MPM, is downregulated by promoter methylation in approximately 90% of MPM cases [16].

Blood examinations are less-invasive diagnostic methods and several serum biomarkers such as mesothelin, osteopontin, CYFRA21-1, and Fibulin-3 have been reported for the diagnosis of MPM [10,17–19]. Among them, mesothelin has been well-studied and is currently considered to be the best serum biomarker of MPM available, although a recent systematic review of medical literature revealed a limited sensitivity [20]. The presence of nucleic acids in the blood was recognized more than 30 years ago [21]. Solid malignant tumors are known to release a significant amount of genomic DNA into the systemic circulation probably through cellular necrosis and apoptosis [21,22]. Therefore, cell-free circulating DNA in the serum or plasma is considered to be a source of useful biomarker during carcinogenesis [23,24], although tumor-derived circulating DNAs are fragmented and present in the blood flow amidst a high background of normal cell-derived DNAs [22,25]. Highly sensitive assays are required to detect tumor-specific genetic alterations in serum-circulating DNAs in patients with malignant tumors [23].

Digital PCR assays have been developed as a highly sensitive assay for the detection of rare genetic abnormalities amidst a high normal background. Digital PCR was originally developed as a tool for the amplification of individual molecules for purposes of identifying and counting individual DNA molecule sequence alterations [26], and now is applied to determine coding mutations, loss of heterozygosity, allelic imbalance and SNP polymorphisms [27,28]. This principle has been also applied to DNA methylation analyses [29]. One of advantages of digital PCR is the sequestration of competing background molecules into negative wells that do not participate in the PCR amplification, leading to improve the ratio of template-to-background in the positive wells [29]. Particularly, competition for primer annealing by background DNA is a major problem in the detection of low-abundance methylation variants by MSP, because sequence redundancy is increased in bisulfite converted DNA, which contains only three bases outside of sites of DNA methylation [29]. To the best of our knowledge, the digital PCR assay for the detection of methylation of miR genes has never been applied as a blood detection test for MPM.

To establish a new detection system for MPM, we developed a digital MSP assay to evaluate the degree of miR-34b/c methylation in serum-circulating DNAs in patients with MPM, comparing those in patients with BAP, and healthy volunteers (HVs).

2. Materials and methods

2.1. Sample collection

We obtained more than 2 mL of peripheral blood samples from 48 MPM cases, 21 BAP cases, and 41 HVs at Okayama University Hospital, Okayama Rosai Hospital, and the National Hospital Organization Yamaguchi Ube Medical Center between August 2006 and August 2011. The characteristics of all 110 cases are shown in Table 1. The blood samples were centrifuged at 3500 rpm for 5 min within 1 h after the collection, and the sera were collected and stored in aliquots at −80 °C at each institute until further experiments. As a positive control (POC), the supernatant of a culture medium for NCI-H290 (H290), an MPM cell line harboring heavy methylation of miR-34b/c [16], was collected and stored at −80 °C. We also collected the supernatant of culture medium for LP9, a non-malignant peritoneal mesothelial cell line, as a negative control. H290 was a kind gift from Dr. Adi F. Gazdar (Hamon Center for Therapeutic Oncology Research and Department of Pathology, University of Texas Southwestern Medical Center at Dallas, Dallas, TX). We purchased LP9 from the Coriell Cell Repository (Camden, NJ). Informed consent was obtained from each case at each institute. The study was approved by the ethics committee of Okayama University (approval number for the genome study, 173).

2.2. DNA extraction and bisulfite conversion

We extracted DNA from 1 mL of serum sample or supernatant of cell culture medium using the QIAamp Circulating Nucleic Acid Kit (Qiagen, Carlsbad, CA), according to the manufacturer's recommendations, and eluted the DNA in 120 μL of the kit's elution buffer. The DNA concentration was quantified using NanoDrop ND-1000

Table 1
Patient characteristics of all samples.

	Subsets		MPM (n = 48)		BAP (n = 21)		HV (n = 41)	
			n	%	n	%	n	%
Age	(69, 38–91)	<69	28	58	4	20	23	56
	(median, range)	≥69	20	42	17	80	18	44
Sex	Male		45	94	15	71	23	56
	Female		3	6	6	29	18	44
Smoking	Never		14	29	9	43	23	56
	Ever		34	71	12	57	18	44
Histology	Epithelioid		36	75	–	–	–	–
	Biphasic		8	17	–	–	–	–
	Sarcomatoid		4	8	–	–	–	–
Clinical stage	I		12	25	–	–	–	–
	II		5	10	–	–	–	–
	III		16	33	–	–	–	–
	IV		12	25	–	–	–	–
	Unknown		3	7	–	–	–	–

MPM, malignant pleural mesothelioma; BAP, benign pleural asbestosis; HV, healthy volunteer.

(NanoDrop Technologies, Wilmington, DE) and the mean dosage of the extracted serum DNA was 4.8 ± 1.8 μg (40 ± 15 ng/μL). Among the 120 μL of extracted serum DNA, 20 μL of DNA (0.8 ± 0.3 μg) was used for bisulfite conversion using the Epitect Bisulfite Kit (Qiagen) and the DNA was eluted in 40 μL of the kit's elution buffer and used as the templates for the assays described below. As for the H290 and LP9 cell lines, the concentrations of extracted DNA from the supernatant of cell culture medium were adjusted to 40 ng/μL. Twenty microliters (0.8 μg) were applied for bisulfite conversion using Epitect Bisulfite Kits (Qiagen) with 40 μL of the final elution.

2.3. Real-time methylation specific PCR (MSP) assay

We designed three sets of MSP primers for the predicted bisulfite-modified sequences based on the nucleotide sequence submitted to GenBank (gene accession numbers, NR_029839 for miR-34b and NR_035765 for miR-34c) and our previous report [16]. Among them, we decided to use the following primer set because of its high sensitivity (data not shown): forward primer, CGTACGGGGTCGAGAGAGT; reverse primer, CTCGACCCGAACTCCCACT. The length of the PCR product was 83 bp. A real-time MSP assay was performed using the StepOnePlus™ Real-Time PCR System (Applied Biosystems) in a final volume of 20 μL per well containing 1 μL of bisulfited DNA (20 ± 7.5 ng/well for serum and 20 ng/well for cell supernatant), 10 μL of 2 × Power SYBR® Green PCR Master Mix (Applied Biosystems), and 0.3 μL of both 10 μM forward and reverse primers. The PCR conditions were as follows: an initial denaturation step at 95 °C for 10 min, followed by 50 cycles of 94 °C for 15 s and 60 °C for 60 s. After PCR amplification, the melting temperature (Tm) of each PCR product was examined using a melting curve analysis.

2.4. Statistical analysis

Differences in the number of miR-34b/c methylated wells were compared between two categorized groups using the Mann–Whitney test. *P* values less than 0.05 were considered statistically significant. The receiver–operating characteristic (ROC) curve analysis was performed to determine the cut-off point for the number of miR-34b/c methylated wells. *P* values less than 0.05 were considered statistically significant.

3. Results

3.1. Detection of positive wells containing miR-34b/c methylated DNA using a melting curve analysis

The fluorescent signal after PCR amplification was detected in all the wells, including those containing a water blank, because of nonspecific PCR reactions. To detect the positive wells containing miR-34b/c methylated DNA, we defined the positive range of the Tm value for miR-34b/c methylation. We investigated the Tm values of 40 wells of the POC samples, 40 wells of LP9 supernatant samples (negative control), and 40 wells containing a water blank. The supernatants of the culture medium for the cell lines contained cell-derived DNA from apoptotic cells and were used as models of the serum samples. The range of the Tm values differed between the 40 POC wells (mean ± standard deviation [SD], 78.25 ± 0.18 °C) and the 40 water blank wells (75.01 ± 0.47 °C) (Fig. 1). In addition, the length of the PCR product of the water blank was confirmed to be shorter than that of POC using gel electrophoresis (Supplemental Figure 1). Furthermore, the Tm values of 39 out of 40 of the wells of the LP9 supernatant sample (negative control) were within the range of the WB samples (Fig. 1). We confirmed that none of the CpG sites that our MSP assay could detect were methylated in the LP9 cell lines using bisulfite sequencing (data not shown). According to this result, we defined the positive range of the Tm values for miR-34b/c methylated wells as 77.71–78.79 °C, which was within the mean Tm values ±3 SDs of 40 wells of the POC samples.

Supplementary material related to this article can be found, in the online version, at http://dx.doi.org/10.1016/j.lungcan.2013.09.017.

3.2. Digital MSP assay for miR-34b/c methylation

In the preliminary study, we examined miR-34b/c methylation in 1 μL of bisulfited DNA from serum-circulating DNA using a real-time MSP assay (one well per sample). miR-34b/c methylation was not present in 1 μL of bisulfited DNA from serum-circulating DNA from the MPM cases, even though the primary tumor harbored heavy miR-34b/c methylation. Considering the dilution effect of tumor-derived DNA in serum-circulating DNA, we repeated the real-time MSP assay for the same serum-circulating DNA and found that miR-34b/c methylation could occasionally be detected. Based on these findings, we decided to perform a real-time MSP assay for 40 PCR wells per serum-circulating DNA sample using the whole elution of bisulfited DNA (40 μL). The quantification of miR-34b/c methylation was performed using a digital MSP assay by counting the number of miR-34b/c methylated wells per sample. For this purpose, a total of 800 μL of PCR mixture containing 40 μL bisulfited DNA templates were first made, and we then distributed them in 20-μL aliquots per well for a total of 40 wells. After PCR amplification, the Tm value of each PCR product was calculated using a melting curve analysis, and the miR-34b/c methylation status of each PCR well was classified according to the positive range of the Tm values for miR-34b/c methylation. In every experiment, a POC sample was placed into a 96-well polypropylene PCR plate to confirm that the Tm value of the POC sample fell within the positive range for miR-34b/c methylation.

3.3. Quantification of miR-34b/c methylation using a digital PCR assay

A distribution map showing the Tm values for all the wells in all the cases was shown in Fig. 1. Each group showed a characteristic distribution of Tm values. Biphasic peaks of Tm values were seen for the MPM and BAP cases, in which the low- and high-grade Tm values were comparable to those of the water blank (low-grade) and the POC of miR-34b/c methylation (high-grade), respectively.

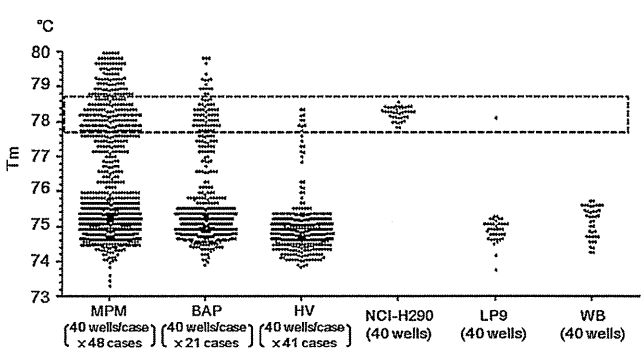

Fig. 1. A distribution map showing the Tm values for all wells in all the cases and the positive range for miR-34b/c-methylated well. The mean Tm values of 40 positive control (POC) wells were 78.25 ± 0.18 °C (mean ± standard deviation [SD]). We defined the well having the Tm within the mean value ± 3 SDs of POC (77.71–78.79 °C) as the positive well for miR-34b/c methylation, indicated with dotted square. MPM, malignant pleural mesothelioma; BAP, benign asbestos pleurisy; HV, healthy volunteers; WB, water blank.

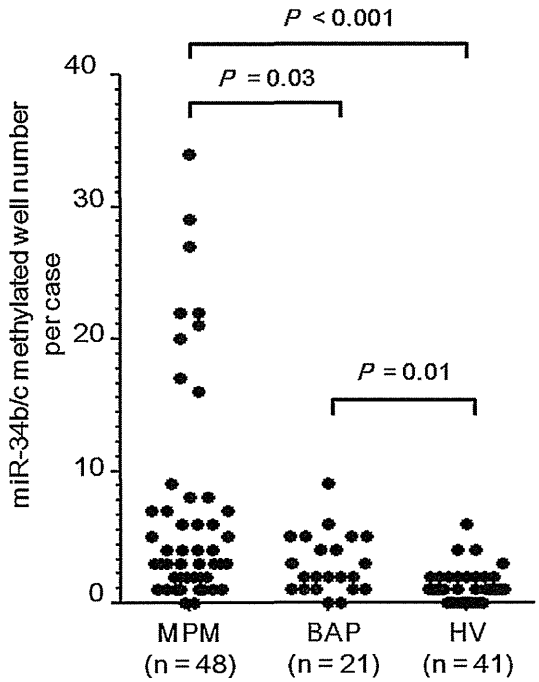

Fig. 2. Comparison of the numbers of miR-34b/c methylated wells. The numbers of miR-34b/c methylated wells were significantly higher in malignant pleural mesothelioma cases than in benign asbestos pleurisy (BAP) cases ($P=0.03$) and healthy volunteers (HVs) ($P<0.001$). BAP cases also showed significantly more miR-34b/c methyled wells than HV ($P=0.01$).

The Tm values of the HVs were mainly around that of the water blank.

The numbers of miR-34b/c methylated wells in the MPM cases was significantly higher than those in the BAP cases ($P=0.03$) or the HVs ($P<0.001$) (Fig. 2). The BAP cases also had significantly higher numbers of miR-34b/c methylated wells than the HVs ($P=0.01$).

3.4. Association between the numbers of miR-34b/c methylated wells and patient characteristics

We evaluated the association between the numbers of miR-34b/c methylated wells per sample and clinicopathological factors. No significant differences in the numbers of miR-34b/c methylated wells were seen when compared according to age, sex, smoking status, and histological subtype. MPM cases with an advanced clinical stage tended to exhibit higher numbers of miR-34b/c methylated wells than those with an early clinical stage except in two cases (Supplemental Figure 2). These two MPM cases with clinical stage I had over 20 miR-34b/c methylated wells; one of the patients had 34 miR-34b/c methylated wells, while the other had 22 miR-34b/c methylated wells and he suffered from a rapid increase in the thickness of the pleura immediately after the initial diagnosis and collection of the serum sample, although the patient was subsequently lost to follow-up.

Supplementary material related to this article can be found, in the online version, at http://dx.doi.org/10.1016/j.lungcan.2013.09.017.

3.5. Optimal cut-off point for miR-34b/c methylation by ROC curve analysis

In order to determine the cut-off number of miR-34b/c methylated wells for MPM cases, we carried out ROC curve analysis comparing MPM cases versus other non-malignant cases (Fig. 3 and

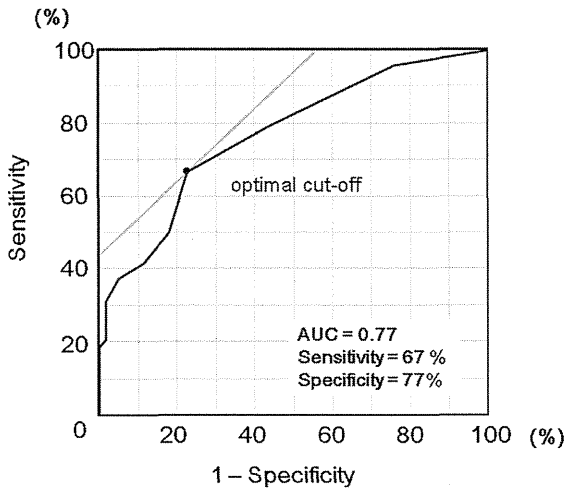

Fig. 3. Receiver–operating characteristic (ROC) curve for the cut-off number of miR-34b/c methylated wells in malignant pleural mesotheliomas. The optimal cut-off for the test is the point closest to the upper-left corner of the graph, which corresponds to miR-34b/c methylation. Area under the ROC curve (AUC) was 0.77.

Supplemental Table 1). According the ROC curve for all cases, three number of methylated wells was the best cut-off of positivity of MPM with a 67% of sensitivity and a 77% specificity for prediction. The area under the ROC curve (AUC) was 0.77.

Supplementary material related to this article can be found, in the online version, at http://dx.doi.org/10.1016/j.lungcan.2013.09.017.

4. Discussion

In this study, we established a highly sensitive assay for the quantification of miR-34b/c methylation in serum-circulating DNA to distinguish MPM cases from BAP cases or HVs. Our assay showed that the degree of miR-34b/c methylation was significantly higher in serum-circulating DNA from MPM cases than from BAP cases or HVs. MPM cases with an advanced clinical stage tend to have more miR-34b/c methylated wells than those with early stage disease, although two early-stage MPM cases did show heavy miR-34b/c methylation of their serum-circulating DNAs.

The dosage of DNA in the blood circulation itself is associated with tumor progression in patients with malignant tumors [30]. Needless to say, the degree of tumor-specific alterations in serum-circulating DNA can be considered a more specific marker for the detection of malignant tumors than the amount of total serum-circulating DNA. PCR reactions for the detection of these tumor-specific alterations in serum-circulating DNA can be interrupted not only by the fragmentation of DNA derived from tumor cells, but also by a high background of DNA derived from non-malignant cells. To overcome these difficulties, several sensitive assays have been developed [29,31,32]. Among them, digital PCR has been established as a highly sensitive assay for the detection of minor genetic alterations among a vast number of normal alleles [27,29]. Digital PCR can also calculate the dosage of the genetic alteration in a sample by determining the percentage of PCR wells with a positive reaction [29], with more precise quantification enabled by analysis of more PCR wells per sample. Of note, although we used TaqMan-based real-time PCR assays in our preliminary experiment, its sensitivity was low and we finally selected the present method (data not shown).

Our results showed that more than three miR-34b/c methylated wells yielded the highest discriminative ability with a 67%

sensitivity and a 77% specificity for predicting the presence of MPM. The AUC was 0.77, indicating that the established assay had a moderate diagnostic accuracy for predicting the occurrence of MPM [33,34]. As a positive test, a high specific threshold is typically required, and if we opt for a specificity of 95% (i.e., a false-positive rate of one out of 20), a sensitivity of our assay results in 38%. For a negative test result to aid in excluding diagnosis, a high sensitive threshold is generally required. At a selected sensitivity of 95%, the specificity of this assay was 24%. These results suggested that the sensitivity and specificity of our assay is almost similar to those of serum mesothelin level in an individual patient data meta-analysis (AUC = 0.77, a sensitivity of 32% at 95% specificity) [20]. With regard to our sensitive assay, false positive cases are present in 43% of BAP cases and 12% of HVs using a cut-off value of three methylated wells. Further investigation is warranted for improvement of both sensitivity and specificity by combining with other biomarkers.

Two early-stage MPM cases exhibited heavy miR-34b/c methylation, indicating that our sensitive assay might detect miR-34b/c methylation during the early stage of MPM pathogenesis. Obviously, the limitation of clinical staging based on conventional radiological examinations should be considered, since one case experienced the rapid progression of the MPM soon after the initial diagnosis. The serum level of miR-34b/c methylation might reflect biological malignancy much more accurately than clinical staging. Further investigations of large-scaled studies are needed to clarify this issue. The sequential occurrence of other malignant tumors is another consideration, since miR34-b/c methylation can be observed in patients with other malignant tumors, such as lung [35,36], colorectal [15], and gastric cancers [37]. Regarding this issue, these malignant tumors were not obviously coincidental in any case of this study.

In conclusion, our digital MSP assay can quantify miR-34b/c methylation in serum-circulating DNA, revealing that miR-34b/c methylation is more heavily and frequently present in serum-circulating DNA from MPM cases than from BAP cases or HVs. This approach might be useful for the establishment of a new detection system for MPM.

Conflict of interest statement

The authors disclose no potential conflicts of interest. We have received Grant-in-Aids for the Okayama-Ken Tokubetsu Dengen Syozai Ken Kagaku Gijyutsu Sinkou Jigyou Kenkyu. Itaku, 2010–2012 (S. Toyooka and T. Otsuki), for Scientific Research from the Ministry of Education, Science, Sports, Culture and Technology of Japan (23791570 for H. Asano), and for the 13 fields of occupational injuries and illnesses of the Japan Labor Health and Welfare Organization (T. Kishimoto).

Acknowledgement

We give special thanks to Yoko Kojima, Research Center for Asbestos-related Disease, Okayama Rosai Hospital for technical support.

References

[1] La Vecchia C, Boffetta P. Role of stopping exposure and recent exposure to asbestos in the risk of mesothelioma. Eur J Cancer Prev 2012;21:227–30.
[2] Robinson BW, Lake RA. Advances in malignant mesothelioma. N Engl J Med 2005;353:1591–603.
[3] Tsao AS, Wistuba I, Roth JA, Kindler HL. Malignant pleural mesothelioma. J Clin Oncol 2009;27:2081–90.
[4] Fennell DA, Gaudino G, O'Byrne KJ, Mutti L, van Meerbeeck J. Advances in the systemic therapy of malignant pleural mesothelioma. Nat Clin Pract Oncol 2008;5:136–47.
[5] Hooper C, Lee YC, Maskell N. Investigation of a unilateral pleural effusion in adults: British Thoracic Society Pleural Disease Guideline 2010. Thorax 2010;65(Suppl. 2):ii4–17.
[6] Scherpereel A, Astoul P, Baas P, Berghmans T, Clayson H, de Vuyst P, et al. Guidelines of the European Respiratory Society and the European Society of Thoracic Surgeons for the management of malignant pleural mesothelioma. Eur Respir J 2010;35:479–95.
[7] Ray M, Kindler HL. Malignant pleural mesothelioma: an update on biomarkers and treatment. Chest 2009;136:888–96.
[8] Davies HE, Nicholson JE, Rahman NM, Wilkinson EM, Davies RJ, Lee YC. Outcome of patients with nonspecific pleuritis/fibrosis on thoracoscopic pleural biopsies. Eur J Cardiothorac Surg 2010;38:472–7.
[9] Creaney J, Olsen NJ, Brims F, Dick IM, Musk AW, de Klerk NH, et al. Serum mesothelin for early detection of asbestos-induced cancer malignant mesothelioma. Cancer Epidemiol Biomarkers Prev 2010;19:2238–46.
[10] van der Bij S, Schaake E, Koffijberg H, Burgers JA, de Mol BA, Moons KG. Markers for the non-invasive diagnosis of mesothelioma: a systematic review. Br J Cancer 2011;104:1325–33.
[11] Kimura K, Toyooka S, Tsukuda K, Yamamoto H, Suehisa H, Soh J, et al. The aberrant promoter methylation of BMP3b and BMP6 in malignant pleural mesotheliomas. Oncol Rep 2008;20:1265–8.
[12] Tomii K, Tsukuda K, Toyooka S, Dote H, Hanafusa T, Asano H, et al. Aberrant promoter methylation of insulin-like growth factor binding protein-3 gene in human cancers. Int J Cancer 2007;120:566–73.
[13] Toyooka S, Carbone M, Toyooka KO, Bocchetta M, Shivapurkar N, Minna JD, et al. Progressive aberrant methylation of the RASSF1A gene in simian virus 40 infected human mesothelial cells. Oncogene 2002;21:4340–4.
[14] Ambros V. MicroRNA pathways in flies and worms: growth, death, fat, stress, and timing. Cell 2003;113:673–6.
[15] Toyota M, Suzuki H, Sasaki Y, Maruyama R, Imai K, Shinomura Y, et al. Epigenetic silencing of microRNA-34b/c and B-cell translocation gene 4 is associated with CpG island methylation in colorectal cancer. Cancer Res 2008;68:4123–32.
[16] Kubo T, Toyooka S, Tsukuda K, Sakaguchi M, Fukazawa T, Soh J, et al. Epigenetic silencing of microRNA-34b/c plays an important role in the pathogenesis of malignant pleural mesothelioma. Clin Cancer Res 2011;17:4965–74.
[17] Grigoriu BD, Scherpereel A, Devos P, Chahine B, Letourneux M, Lebailly P, et al. Utility of osteopontin and serum mesothelin in malignant pleural mesothelioma diagnosis and prognosis assessment. Clin Cancer Res 2007;13:2928–35.
[18] Cube M, Taeger D, Weber DG, Pesch B, Brand P, Johnen G, et al. Performance of biomarkers SMRP, CA125, and CYFRA 21-1 as potential tumor markers for malignant mesothelioma and lung cancer in a cohort of workers formerly exposed to asbestos. Arch Toxicol 2011;85:185–92.
[19] Pass HI, Levin SM, Harbut MR, Melamed J, Chiriboga L, Donington J, et al. Fibulin-3 as a blood and effusion biomarker for pleural mesothelioma. N Engl J Med 2012;367:1417–27.
[20] Hollevoet K, Reitsma JB, Creaney J, Grigoriu BD, Robinson BW, Scherpereel A, et al. Serum mesothelin for diagnosing malignant pleural mesothelioma: an individual patient data meta-analysis. J Clin Oncol 2012;30:1541–9.
[21] Leon SA, Shapiro B, Sklaroff DM, Yaros MJ. Free DNA in the serum of cancer patients and the effect of therapy. Cancer Res 1977;37:646–50.
[22] Jahr S, Hentze H, Englisch S, Hardt D, Fackelmayer FO, Hesch RD, et al. DNA fragments in the blood plasma of cancer patients: quantitations and evidence for their origin from apoptotic and necrotic cells. Cancer Res 2001;61:1659–65.
[23] Gormally E, Caboux E, Vineis P, Hainaut P. Circulating free DNA in plasma or serum as biomarker of carcinogenesis: practical aspects and biological significance. Mutat Res 2007;635:105–17.
[24] Paci M, Maramotti S, Bellesia E, Formisano D, Albertazzi L, Ricchetti T, et al. Circulating plasma DNA as diagnostic biomarker in non-small cell lung cancer. Lung Cancer 2009;64:92–7.
[25] Horlitz M, Lucas A, Sprenger-Haussels M. Optimized quantification of fragmented, free circulating DNA in human blood plasma using a calibrated duplex real-time PCR. PLoS One 2009;4:e7207.
[26] Vogelstein B, Kinzler KW. Digital PCR. Proc Natl Acad Sci USA 1999;96:9236–41.
[27] Pohl G, Shih Ie M. Principle and applications of digital PCR. Expert Rev Mol Diagn 2004;4:41–7.
[28] Yung TK, Chan KC, Mok TS, Tong J, To KF, Lo YM. Single-molecule detection of epidermal growth factor receptor mutations in plasma by microfluidics digital PCR in non-small cell lung cancer patients. Clin Cancer Res 2009;15:2076–84.
[29] Weisenberger DJ, Trinh BN, Campan M, Sharma S, Long TI, Ananthnarayan S, et al. DNA methylation analysis by digital bisulfite genomic sequencing and digital MethyLight. Nucleic Acids Res 2008;36:4689–98.
[30] Sirera R, Bremnes RM, Cabrera A, Jantus-Lewintre E, Sanmartin E, Blasco A, et al. Circulating DNA is a useful prognostic factor in patients with advanced non-small cell lung cancer. J Thorac Oncol 2011;6:286–90.
[31] Li L, Choi JY, Lee KM, Sung H, Park SK, Oze I, et al. DNA methylation in peripheral blood: a potential biomarker for cancer molecular epidemiology. J Epidemiol 2012;22:384–94.
[32] Snell C, Krypuy M, Wong EM, Loughrey MB, Dobrovic A. BRCA1 promoter methylation in peripheral blood DNA of mutation negative familial breast cancer patients with a BRCA1 tumour phenotype. Breast Cancer Res 2008;10:R12.
[33] Shen J, Todd NW, Zhang H, Yu L, Lingxiao X, Mei Y, et al. Plasma microRNAs as potential biomarkers for non-small-cell lung cancer. Lab Invest 2011;91:579–87.

[34] Fischer JE, Bachmann LM, Jaeschke R. A readers' guide to the interpretation of diagnostic test properties: clinical example of sepsis. Intensive Care Med 2003;29:1043–51.
[35] Tanaka N, Toyooka S, Soh J, Kubo T, Yamamoto H, Maki Y, et al. Frequent methylation and oncogenic role of microRNA-34b/c in small-cell lung cancer. Lung Cancer 2012;76:32–8.
[36] Wang Z, Chen Z, Gao Y, Li N, Li B, Tan F, et al. DNA hypermethylation of microRNA-34b/c has prognostic value for stage non-small cell lung cancer. Cancer Biol Ther 2011;11:490–6.
[37] Suzuki H, Yamamoto E, Nojima M, Kai M, Yamano HO, Yoshikawa K, et al. Methylation-associated silencing of microRNA-34b/c in gastric cancer and its involvement in an epigenetic field defect. Carcinogenesis 2010;31:2066–73.

We chose to use AMPLATZER II plugs embedded with Onyx to stop this patient's bile leak. Onyx was selected instead of NBCA because NBCA had been used multiple times in this patient, to no avail, and previous studies have suggested that NBCA fails to permanently occlude leaks that communicate with the main biliary tree (3). In addition, Onyx could be injected at a slower pace than glue; the higher-viscosity formulation was chosen, even though Onyx-18 might have functioned equally. The combination of Onyx baffled by AMPLATZER Vascular Plugs proved successful in sealing this patient's refractory biliary leak. Although one downstream plug might have been sufficient, we used both to trap the liquid embolic agent to avoid the possibility of its later migration into the biliary tree. We believe this technique of combining a metallic with a liquid occlusion agent may provide an appealing permanent alternative to NBCA embolization within the biliary tree, and may warrant further use.

REFERENCES

1. Carrafiello G, Ierardi AM, Piacentino F, Cardim LN. Percutaneous transhepatic embolization of biliary leakage with n-butyl cyanoacrylate. Indian J Radiol Imaging 2012; 22:19–22.
2. Schirmer CM, Hoit DA, Malek AM. Amplatzer-Onyx sandwich: a method for impermeable proximal cerebral vessel occlusion. J Vasc Interv Radiol 2008; 19:459–460.
3. Vu DN, Strub WM, Nguyen PM. Biliary duct ablation with N-butyl cyanoacrylate. J Vasc Interv Radiol 2006; 17:63–69.
4. Schild HH, Meyer C, Mohlenbroch M, Mueller SC, Simon B, Kuhl CK. Transrenal ureter occlusion with an Amplatzer Vascular Plug. J Vasc Interv Radiol 2009; 20:1390–1392.
5. Shabrang C, Kelbach SM, Hsu DP, Zippe CD, Lie KT. Therapeutic ureteral occlusion with n-butyl cyanoacrylate glue and an AMPLATZER Plug scaffold. J Vasc Interv Radiol 2012; 23:428–430.

Bleeding into a Pulmonary Cyst Caused by Pulmonary Radiofrequency Ablation

From: Ryotaro Kishi, MD
Hidefumi Mimura, MD
Takao Hiraki, MD
Hideo Gobara, MD
Mayu Uka, MD
Shinichi Toyooka, MD
Susumu Kanazawa, MD
Departments of Radiology (R.K., H.M., T.H., H.G., M.U., S.K.) and Cancer and Thoracic Surgery (S.T.)
Okayama University Medical School
2-5-1 Shikata-cho, Kita-ku
Okayama 700-8558, Japan

Editor:

Pneumothorax and pleural effusion are common complications after radiofrequency (RF) ablation of lung tumors (1). Massive hemorrhage and hemoptysis are rare but potentially fatal complications (2–4). We report a case of bleeding into a pulmonary cyst caused by pulmonary RF ablation.

Our institutional review board gave us an approval and a waiver of informed consent for the present retrospective study. An 80-year-old woman with a 50-year history of bronchial asthma had undergone right upper lobectomy for lung adenocarcinoma (T1N0M0, stage IA) 7 years previously. Recurrence in the right lower lobe 2 years later was treated with RF ablation. Three years after RF ablation, local recurrence at the same site was treated with further RF ablation. After the second RF ablation treatment, a pulmonary cyst formed at the ablated site. During follow-up, focal thickening of the cyst wall was noted, suggesting local recurrence (**Figure, a**). Positron emission tomography showed high uptake of [^{18}F]fluorodeoxyglucose in the thickened cyst wall. Subsequent computed tomography (CT)–guided biopsy confirmed that this thickening was recurrence of adenocarcinoma. Laboratory test results on admission were unremarkable, with normal hemoglobin, platelet count, and coagulation. Respiratory function testing showed poor pulmonary function, with a vital capacity of 1.04 L and forced expiratory volume in 1 second of 0.91 L. Blood gas analysis showed a partial arterial O_2 pressure of 66.9 mm Hg and a partial arterial CO_2 pressure of 54.4 mm Hg on room air. Treatment with further RF ablation was planned.

Under conscious sedation, the patient was placed in the prone position. RF ablation was performed with use of multitined expandable electrodes (LeVeen; Boston Scientific, Natick, Massachusetts) with 2-cm-diameter arrays under CT fluoroscopic guidance (**Figure, b**). RF energy was applied at four sites for a total of 23 minutes at a maximum power of 50 W. During RF ablation, bleeding into the pulmonary cyst was observed on CT fluoroscopic images, but the patient remained asymptomatic with stable vital signs (**Figure, c**). Immediately after RF ablation, the cyst was punctured with an 18-gauge needle, and 15 mL of blood was aspirated. CT scan 15 minutes after aspiration showed remaining blood in the cyst, but the volume of blood did not increase over time. The patient's vital signs remained stable, and she returned to the ward.

The following day, the patient was found in the ward in respiratory arrest, with a Glasgow coma scale score of 3. Her blood pressure was 185/88 mm Hg, heart rate was 120 beats/min, and O_2 saturation was 40%. She was intubated in the ward and transferred to the intensive care unit. Chest CT showed that the hematoma in the pulmonary cyst had decreased in volume, but ground-glass opacity and consolidation were observed around

None of the authors have identified a conflict of interest.

http://dx.doi.org/10.1016/j.jvir.2013.03.023

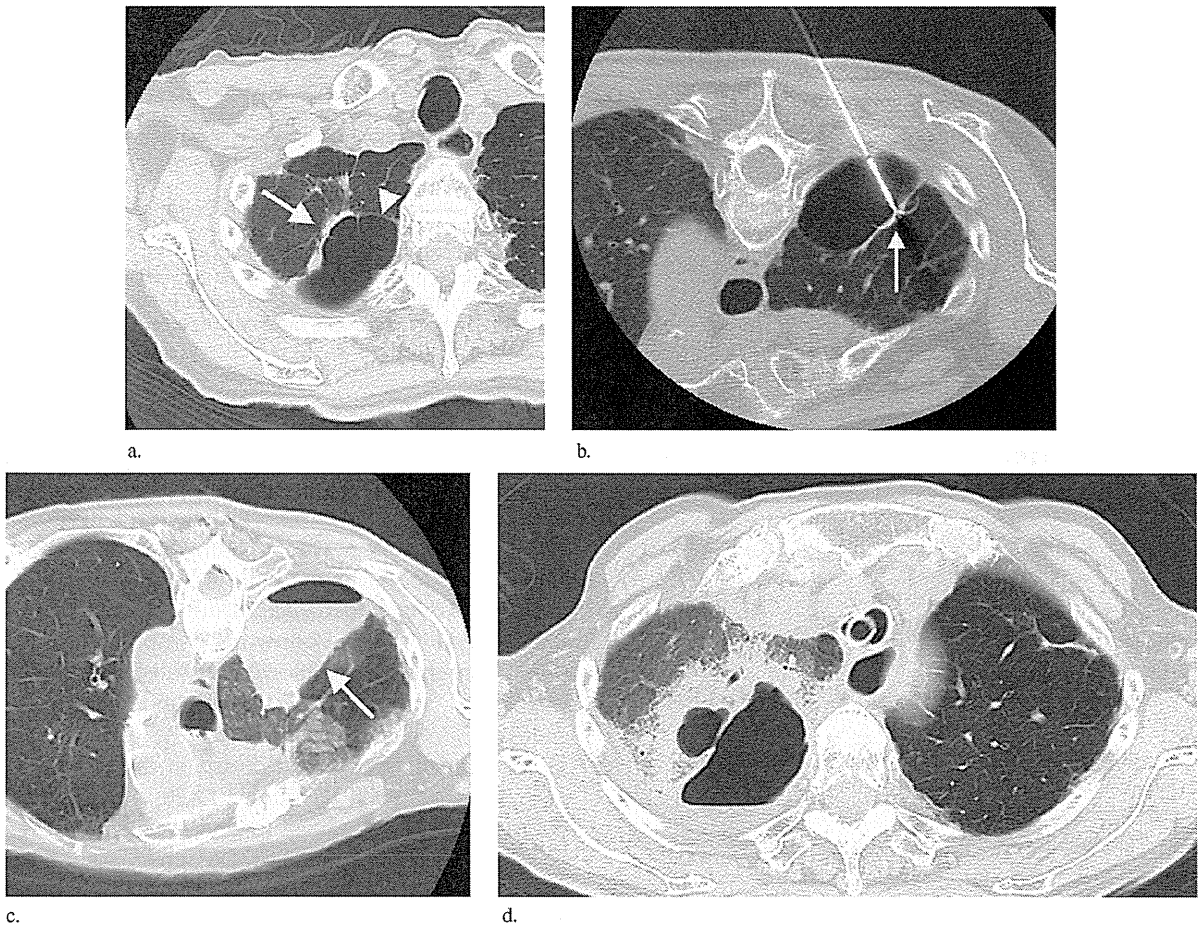

Figure. **(a)** CT image before RF ablation shows the thickened wall (arrow) of the pulmonary cyst (arrowhead) that had formed after previous RF ablation, suggesting cancer recurrence. **(b)** CT image during RF ablation with the patient in the prone position shows the multitined expandable electrode with 2-cm-diameter arrays (arrow). **(c)** CT image immediately after RF ablation shows bleeding (arrow) into the pulmonary cyst. **(d)** CT image the day after RF ablation shows decreased volume of the hematoma in the pulmonary cyst and ground-glass opacity and consolidation around the cyst.

the cyst (**Figure, d**). Mucus plugs were observed in the left lower-lobe bronchi, and there were ground-glass opacities and small nodules scattered throughout the left lower lobe. Bronchoscopy revealed edema of the walls of the left main bronchus and left lower lobe bronchi and hemosputum impacted in the left lower lobe bronchi. There was no active bleeding in the bronchi. The patient recovered to a normal level of consciousness.

Subsequently, the pulmonary cyst became infected, with diffuse thickening of the cyst wall and fluid collection inside the cyst. Sputum culture revealed *Pseudomonas aeruginosa* infection. CT-guided percutaneous drainage of the infected cyst was performed 7 days after RF ablation with the use of a 10-F pigtail catheter (Ureflex; UreSil, Skokie, Illinois). As bronchoscopy revealed a communication between the pulmonary cyst and the bronchus, the affected bronchus was plugged with an Endobronchial Watanabe Spigot (Novatech, Grasse, France) to facilitate lavage of the cyst via the catheter. The patient was treated with various antibiotic agents, and the infection resolved. The spigot and drainage catheter were removed 40 days and 62 days after RF ablation, respectively. The patient was discharged without further sequelae 88 days after RF ablation.

Vaughn et al (2) reported a case in which massive hemorrhage into the lung and pleural cavity after RF ablation led to death on postoperative day 23. The cause of hemorrhage was unknown in that case because the pulmonary and bronchial arteriograms failed to identify a distinct source of bleeding. Massive hemoptysis from a pulmonary artery pseudoaneurysm that formed after RF ablation has also been reported (3,4). It was assumed that the bleeding in these cases was not from the tumor, but from a nearby vessel after the electrode or its tines pierced the vessel or the vessel was thermally damaged. Compared with parenchymal bleeding, bleeding into a cavity is more likely to be massive even in the absence of coagulopathy, because there is less likely to be a tamponade effect. Although the exact cause of respiratory arrest could not be determined in the present case, we speculate that aspiration of blood from the cyst into the bronchus caused bronchial irritation and acute exacerbation of asthma.

Bleeding into the cyst resulted in another serious condition, ie, infection of the cyst, which required prolonged intensive care treatment, including administration of antibiotic agents, percutaneous drainage, and spigot placement in the bronchus.

In summary, we report a case of bleeding into a pulmonary cyst as a result of pulmonary RF ablation. The bleeding subsequently resulted in respiratory arrest. Although the patient was resuscitated, the cyst subsequently became infected, and the patient required prolonged treatment.

REFERENCES

1. Hiraki T, Tajiri N, Mimura H, et al. Pneumothorax, pleural effusion, and chest tube placement after radiofrequency ablation of lung tumors: Incidence and risk factors. Radiology 2006; 241:275–283.
2. Vaughn C, Mychaskiw G, Sewell P. Massive hemorrhage during radiofrequency ablation of a pulmonary neoplasm. Anesth Analg 2002; 94: 1149–1151.
3. Sakurai J, Mimura H, Gobara H, Hiraki T, Kanazawa S. Pulmonary artery pseudoaneurysm related to radiofrequency ablation of lung tumor. Cardiovasc Intervent Radiol 2010; 33:413–416.
4. Yamakado K, Takaki H, Takao M, et al. Massive hemoptysis from pulmonary artery pseudoaneurysm caused by lung radiofrequency ablation: successful treatment by coil embolization. Cardiovasc Intervent Radiol 2010; 33:410–412.

Direct Percutaneous Sac Injection for Treatment of a Thoracic Type II Endoleak

From: Andreas S. Kreusch
Shaun Samuels, MD
James F. Benenati, MD
Melanie Schernthaner, MD
Heiko Uthoff, MD
Baptist Cardiac and Vascular Institute (A.S.K., S.S., J.F.B., M.S., H.U.)
8900 N. Kendall Dr.
Miami, FL 33176; and
Department of Angiology (H.U.)
University Hospital Basel
Basel, Switzerland

Editor:

Thoracic endovascular aneurysm repair has become the treatment of choice for many chronic and acute pathologic processes of the descending thoracic aorta, including treatment of ruptured thoracic aneurysms. Endoleaks remain a nuisance associated with endovascular repair and have been reported in as many as 29% of cases (1). Abdominal direct percutaneous sac injection (DPSI) has been described as a feasible alternative treatment option if a standard transarterial approach is not possible or has previously failed to resolve a type II endoleak (2).

Here we describe an interesting case of evaluation and treatment of a thoracic endoleak with the use of a direct percutaneous approach for selective bronchial artery and aneurysm sac embolization.

A 77-year-old man with a history of open ascending aortic aneurysm repair and aortic bioprosthetic valve replacement initially presented with an upper descending thoracic aortic dissection (Stanford type B, DeBakey type III), which had ruptured into the mediastinum. The patient underwent emergent percutaneous endograft repair. Despite deployment of four EXCLUDER endografts (W.L. Gore and Associates, Flagstaff, Arizona) a small type IA endoleak persisted and could not be treated by using a standard femoral approach as a result of a highly tortuous thoracic aorta. By using a transapical access as a "bailout" approach, the type I endoleak was excluded successfully with deployment of a Palmaz 5010 stent. Follow-up computed tomographic (CT) angiography at 6 months revealed contrast medium within the aneurysm sac, likely indicating a type II endoleak superior and posterior to the aortic arch (**Figure, a**). The patient was placed prone on the procedure table, and cone-beam CT (Allura FD-20; Philips, Best, The Netherlands) was obtained to determine the best region to be accessed (**Figure, a**, shows planned puncture route). After local anesthesia was obtained, a 22-gauge Chiba needle was advanced on a paraspinal route directly into the thoracic aneurysm sac under fluoroscopy guidance by using landmarks of the thoracic endograft for reference. Bloody backflow indicated successful needle entry into the aneurysm sac, as also confirmed by lateral views. A sac injection was performed with approximately 5 mL of contrast agent to evaluate the aneurysm sac and type of endoleak. A large outflowing bronchial artery was observed, but there was no sign of a concurrent type I endoleak (**Figure, b**). At this time, an AccuStick introducer system (Boston Scientific, Natick, Massachusetts) was used to exchange the needle for a 6-F sheath. A 0.018-inch, 70° gold-tip angled Glidewire (Terumo, Somerset, New Jersey) was used for selective probing of the bronchial artery, and a 2.4-F Progreat microcatheter (Terumo) was advanced. Coil embolization with six 3–4-mm × 2-cm Tornado microcoils (Cook, Bloomington, Indiana) was performed. A slurry of Gelfoam (Baxter, Deerfield, Illinois) mixed in 50/50 contrast medium along with 225 U of thrombin was then carefully injected into the aneurysm sac until stasis within the sac was observed (**Figure, c**). The catheter was removed, and manual pressure was applied at the puncture site to achieve hemostasis. Five-week and 6-month CT follow-up demonstrated no signs of recurrent endoleak, with shrinkage of the aneurysm sac (maximal axial diameter before intervention, 80.2 mm; after 6 mo, 47.2 mm) and mediastinal hematoma (**Figure, d**).

None of the authors have identified a conflict of interest.

http://dx.doi.org/10.1016/j.jvir.2013.03.024